UNIVERSITY OF SÃO PAULO
SÃO CARLOS INSTITUTE OF PHYSICS

FLÁVIA MAYUMI ODAHARA DE ABREU

Prospecting the interaction interface in the polymerization process of the enzyme glutaminase C

São Carlos
2023

FLÁVIA MAYUMI ODAHARA DE ABREU

Prospecting the interaction interface in the polymerization process of the enzyme glutaminase C

Dissertation presented to the Graduate Program in Physics at the São Carlos Institute of Physics, University of São Paulo to obtain the degree of Master of Science.

Concentration area: Applied Physics
Option: Biomolecular Physics

Advisor: Prof. Dr. Andre Luis Berteli Ambrosio

Original Version

São Carlos
2023

Abreu, Flávia Mayumi Odahara de
Prospecting the interaction interface in the polymerization process of the enzyme glutaminase C / Flávia Mayumi Odahara de Abreu; advisor Andre Luis Berteli Ambrosio -- São Carlos 2023.
71 p.

Dissertation (Master's degree - Graduate Program in Biomolecular Physics) -- Instituto de Física de São Carlos, Universidade de São Paulo - Brasil , 2023.

1. Glutamine. 2. Neoplasia. 3. Cancer. 4. Enzymes. 5. Structural biology. I. Ambrosio, Andre Luis Berteli, advisor. II. Title.

FOLHA DE APROVAÇÃO

Flávia Mayumi Odahara de Abreu

Dissertação apresentada ao Instituto de Física de São Carlos da Universidade de São Paulo para obtenção do título de Mestra em Ciências. Área de Concentração: Física Biomolecular.

Aprovado (a) em: 30/10/2023

Comissão Julgadora

Dr(a).: Andre Luis Berteli Ambrosio

Instituição: (IFSC/USP)

Dr(a).: Leonardo Talachia Rosa

Instituição: (UNICAMP/Campinas)

Dr(a).: José Luiz de Souza Lopes

Instituição: (FFCLRP/USP)

With love,
to my family, the most precious thing in my life.

ACKNOWLEDGMENTS

Words fall short in capturing the depth of my gratitude for those who have walked alongside me during this transformative journey. This has been the most daunting yet exhilarating chapter of my life, and I owe the experience to each of you. I find myself blessed beyond measure to be surrounded by such extraordinary people.

First and foremost, I thank God for His incredible blessings.

The compass guiding me through every moment leading to this point has been the unwavering support of my family. And to mom, dad, Vanessa, and Lívia – your visits, calls, and trips between Araçatuba and São Carlos brought unlimited joy and solace, especially when I need it the most. My love for you knows no bounds.

I extend my gratitude, especially, to my beloved grandmother, *vovó Linda*, who has been my pillar of strength from the very beginning. *Vovó*, your unconditional encouragement and celebration of even the smallest achievements have been a beacon in my life. You never had the chance to pursue formal education in university, yet you were an example of wisdom, guided by the grace of God, and nurtured and honest, loving, and caring family. Unfortunately, you could not see me reach the end of this journey; nonetheless, I will always carry you in my heart. I am profoundly grateful for having shared life with you. Hopefully, I can make you proud.

I wish to express my deep gratitude to Professor Andre, who has been the best advisor I could ever ask for. You taught me so much about scientific thinking and equipped me with all the tools I needed to navigate this project. Seeing your never-ending passion and excitement for science is a source of inspiration. Thank you for taking me as a student, for your all patience and motivation, which were essential in maintaining my enthusiasm. Your mentorship has enabled me to grow professionally and personally, and it has been an honor to work alongside you.

I manifest heartfelt thanks to the friends who have become my family. Letícia, Nícolas, Cris, Lucas, Angélica, and Lucas (Guincho), our bond, forged during our undergraduate years, has only grown stronger with time. You have been my rock in São Carlos. Thank you for allowing me to talk about my problems, worries, for the amazing experiences together, and for the constant reminders to balance my studies with the other good things in life. Josh, you, too, have left a memorable mark on this

journey. Helena, your unwavering belief in me and the clarity during my darkest moments have been invaluable.

To my friends and colleagues from grad school, particularly those in the lab, I would like you to know how deeply I appreciate your company, which made even the most demanding days brighter. The laughter, shared jokes, late night work sessions, holidays and weekends spent in pursuit of knowledge are moments I will treasure forever. And to Gabi, Léo, Lívia, Luana, and Matías, each of you has been vital in this journey. I am grateful for your kindness, patience, guidance, and friendship, especially during the most trying days.

Luiza and Karen, your sweetness is limitless. I am honored to have had the opportunity to support you during your projects at our group. I have no doubt that you will continue to fascinate your future colleagues as you have done for me. Our shared adventures hold great value for me. You, too, have brought joy to my time in the lab and helped me face work with a positive spirit.

Camila and Edwin, your contributions to this work were indispensable. I would have been completely lost at the start without your guidance. And to the visiting students – Sebastián, Ignacio, and Leonardo – you left a lasting mark on me, teaching me important lessons as well.

I also acknowledge with gratitude the essential contributions of our colleagues at the LNNano and LNBio (CNPEM). Moreover, I extend my appreciation for our research group, professors and all the individuals involved in the remarkable work being done at our institution. I am also indebted to IFSC and USP for the steady support, providing the infrastructure and research excellence that made my participation in this postgraduate program possible.

This study was financed by the Coordenação de Aperfeiçoamento de Pessoal de Nível Superior (CAPES) via scholarship 88887.474257/2020-00 to FMOA, by the Fundação de Amparo à Pesquisa do Estado de São Paulo (FAPESP), via grants 2017/11766-5 (to ALBA) and 2013/07600-3 (CIBFAR/CEPID).

“The cure to boredom is curiosity.
There is no cure for curiosity.”
Dorothy Parker

ABSTRACT

ABREU, F. M. O. **Prospecting the interaction interface in the polymerization process of the enzyme Glutaminase C**. 2023. 71 p. Dissertation (Master of Science) – São Carlos Institute of Physics, University of São Paulo, São Carlos, 2023.

The energetic and biosynthetic demands in cancer are linked to the alteration of many pathways in the cell. One of the main changes occurs in glutaminolysis; glutamine is one of the essential nutrients for tumor metabolism and is converted into glutamate by the glutaminase enzymes, encoded in mammals by two distinct genes, *GLS* and *GLS2.* Among the existing isoforms, Glutaminase C (GAC) is crucial and found in abundance in different tumor lineages. It can be found in different oligomeric states with varying efficiency, and the most active type is characterized by the formation of helical filaments (fGAC) in the presence of inorganic phosphate (Pi). However, the molecular mechanism by which oligomerization and increased activity arise is still elusive. Therefore, this project aims to discuss a novel model proposed by our group through the combination of cryo-electron microscopy (cryo-EM) and biochemical studies of the wild-type or modified protein. To this end, site-directed mutagenesis was performed in residues from regions of the suggested interaction interface and activation loop. Wild-type mouse GAC and its mutants were produced by heterologous expression in bacteria on a large scale in soluble fraction and purified in three stages. By dynamic light scattering (DLS) analysis, it was possible to observe a shift from the tetrameric to the filamentous form of the wild-type protein upon addition of Pi, while mutants remained in their initial state under the same conditions. Enzymatic efficiency was confirmed by kinetic assays based on a coupled reaction, tracking the absorbance of 340 nm wavelength light by NADH formed during the conversion of glutamate into α-ketoglutarate by the enzyme glutamate dehydrogenase (GDH). Analysis showed that the mutants also show reduced efficiency in contrast to the wild-type protein even in the presence of Pi. Thus, the data suggest that mutations that prevent filamentation are also responsible for inactivating the protein, confirming that substituted residues are critical for the formation, stabilization, and function of fGAC. We propose a mechanism for the transition from inactive dimers to hyper-active fGAC; understanding this process could establish the enzyme Glutaminase C as a promising molecular target for the development of new anti-tumor therapies.

Keywords: Glutamine. Neoplasia. Cancer. Enzymes. Structural biology.

RESUMO

ABREU, F. M. O. **Prospecção da interface de interação no processo de polimerização da enzima Glutaminase C**. 2023. 71 p. Dissertação (Mestrado em Ciências) – Instituto de Física de São Carlos, Universidade de São Paulo, São Carlos, 2023.

As demandas energéticas e biossintéticas no câncer estão relacionadas à alteração de muitas vias na célula. Uma das principais mudanças ocorre na glutaminólise; a glutamina é um dos nutrientes essenciais para o metabolismo tumoral e é convertida em glutamato pelas enzimas glutaminases, codificadas em mamíferos por dois genes distintos, *GLS* e *GLS2*. Entre as isoformas existentes, a Glutaminase C (GAC) é crucial e encontrada em abundância em diferentes linhagens tumorais. Ela pode ser encontrada em diferentes estados oligoméricos com eficiência variável, e o tipo mais ativo é caracterizado pela formação de filamentos helicoidais (fGAC) na presença de fosfato inorgânico (Pi). No entanto, o mecanismo molecular pelo qual ocorre a oligomerização e o aumento de atividade ainda é desconhecido. Portanto, este projeto tem como objetivo discutir um novo modelo proposto pelo nosso grupo por meio da combinação de estudos de criomicroscopia eletrônica (cryo-EM) e bioquímicos da proteína selvagem ou modificada. Para isso, foi realizada mutagênese sítio-dirigida em resíduos de regiões da interface de interação sugerida e do loop de ativação. A GAC selvagem de camundongo e mutantes foram produzidas por expressão heteróloga em sistema bacteriano em grande escala na fração solúvel e purificadas em três etapas. Por meio da análise por espalhamento dinâmico de luz (DLS), foi possível observar uma transição da forma tetramérica para a forma filamentosa da proteína selvagem após a adição de Pi, enquanto as mutantes permaneceram em seu estado inicial sob as mesmas condições. A eficiência enzimática foi confirmada por ensaios cinéticos baseados em uma reação acoplada, acompanhando a absorbância de luz de comprimento de onda de 340 nm pelo NADH formado durante a conversão de glutamato em α-cetoglutarato pela enzima glutamato desidrogenase (GDH). A análise mostrou que os mutantes também apresentam eficiência reduzida em contraste com a proteína selvagem, mesmo na presença de Pi. Assim, os dados sugerem que as mutações que impedem a formação de filamentos também são

responsáveis pela inativação da proteína, confirmando que os resíduos substituídos são críticos para a formação, estabilização e função de fGAC. Propomos um mecanismo para a transição de dímeros inativos para fGAC hiperativos; entender esse processo poderia estabelecer a enzima Glutaminase C como um alvo molecular promissor para o desenvolvimento de novas terapias antitumorais.

Palavras-chave: Glutamina. Neoplasia. Câncer. Enzimas. Biologia estrutural.

LIST OF FIGURES

LIST OF ABREVIATIONS AND ACRONYMS

α-kg	α-ketoglutarate
ATP	Adenosine triphosphate
BPTES	Bis-2-(5-phenylacetamido-1,3,4-thiadiazol-2-yl)ethyl sulfide
BRAF	V-Raf murine sarcoma viral oncogene homolog B oncogene
CB-839	Telaglenastat glutaminase inhibitor
CNPEM	Centro Nacional de Pesquisa em Energia e Materiais
EGF	Epidermal growth factor
EDTA	Ethylenediaminetetraacetic acid
FPLC	Fast Protein Liquid Chromatography
GDH	Glutamate dehydrogenase
Gln	Glutamine
HIF	Hypoxia-inducible factor
IPTG	Isopropyl-ß-D-thiogalactopyranoside
KRAS	Kirsten rat sarcoma virus
LB	Luria-Bertani
LNBio	Laboratório Nacional de Biologia
LNNano	Laboratório Nacional de Nanotecnologia
mGAC	*Mus musculus* Glutaminase C
MYC	Myc myelocytomatosis oncogene
NAD	Nicotinamide adenine dinucleotide
NaCl	Sodium chloride
NCBI	The National Center for Biotechnology Information
NR	Nuclear receptor
PDB	Protein Data Bank

Pi	Inorganic phosphate
PMSF	Phenylmethylsulfonyl fluoride
RAS	Rat sarcoma virus oncogene
SDS-PAGE	Sodium dodecyl-sulfate polyacrylamide gel electrophoresis
TCEP	Tris(2-carboxyethyl)phosphine
TGF-β	Transforming growth factor β
VEGF	Vascular endothelial growth factor

CONTENTS

1 INTRODUCTION

1.1 Cancer

Cancer research plays a crucial role in addressing one of the most pressuring challenges of our time. A major public health issue, it is the second main cause of death worldwide, with nearly 10 million deaths in 2020 – nearly one in every six deaths –, and countries of low and middle income are the most affected by the burden of the disease.[1] Projections state that cancer will continue to pose a substantial threat to global health, with an estimated 17 million deaths projected by 2030,[2] and may become the leading cause of premature mortality throughout this by 2060.[3] Hence, a thorough comprehension of the disease's mechanisms is essential for developing precise treatments and effectively combating it.

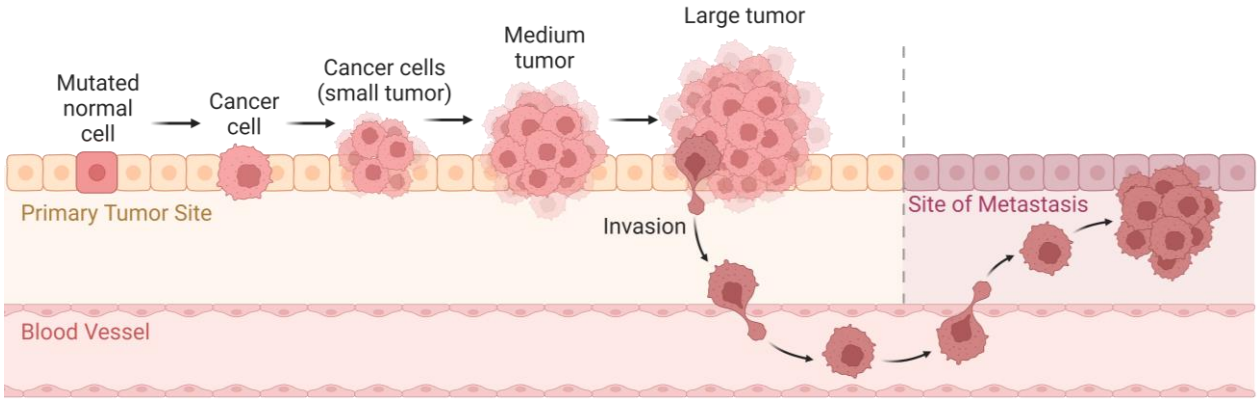

Figure 1 - Stages of cancer progression.

Source: By Prof. Andre Ambrosio, created with BioRender.

Cancer is a multifaceted scenario defined by a heterogeneous group of diseases characterized by molecular complexities. In summary, an uncontrolled growth and proliferation of abnormal cells, also known as a tumor, neoplasm, or a pre-cancerous lesion, can acquire distinct malignant features over time, and potentially invade surrounding tissues and spread to other parts of the body, in a process known as metastasis (Figure 1). The condition, then, is called cancer, and the common biological characteristics contributing to its initiation and progression are known as the “hallmarks of cancer” (Figure 2). These are not all unique to cancer cells but are essential for cancer to develop and progress.[4]

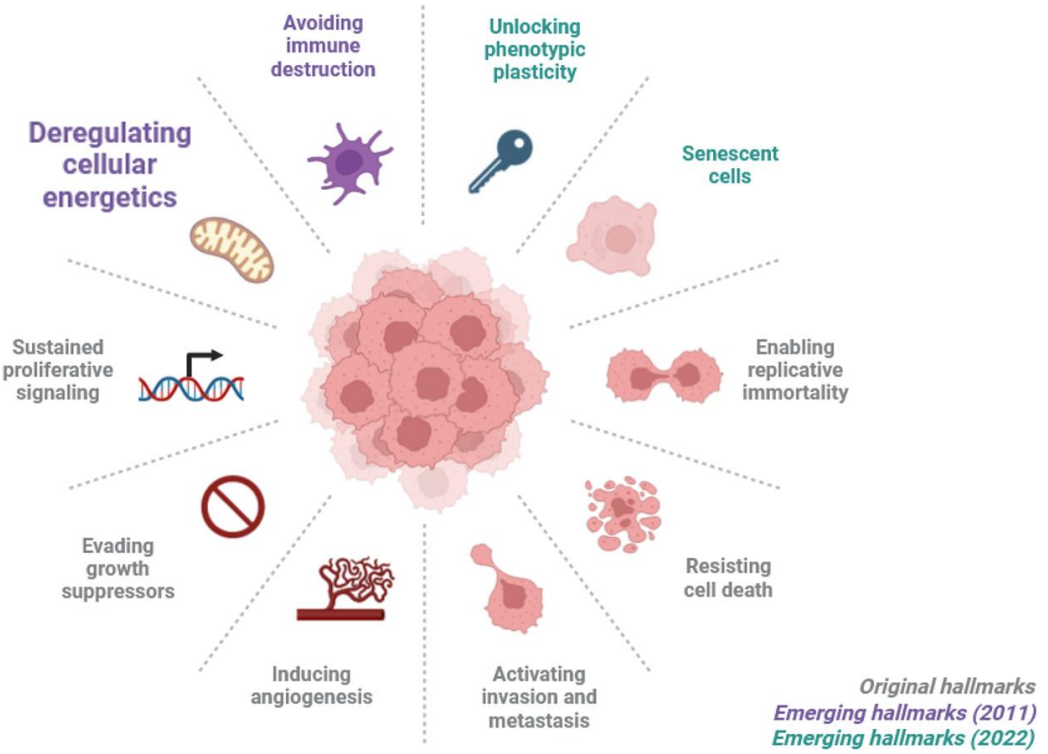

Figure 2 – The 10 hallmarks of cancer. The features proposed by Hanahan and Weinberg[4] define tumor initiation and progression over time. Particularly, deregulating cellular energetics is related to an increase in glucose and glutamine uptake for energetic and biosynthetic demands.

Source: By Prof. Andre Ambrosio, created with BioRender.

They were first proposed by Douglas Hanahan and Robert Weinberg in 2000,[4] and have since then been refined and expanded:[5-6]

I. Sustained proliferative signaling. Cancer cells present self-sufficient cell division, by producing their own growth signals, activating oncogenes, and presenting mutations in growth factor receptors.

II. Replicative immortality. Cancer cells can divide indefinitely, being able to bypass the replication limit present in healthy cells, due to mechanisms including telomerase activation, mutations in tumor suppressor genes (such as p53), or epigenetic changes.

III. Insensitivity to growth suppressor signals, disregarding the normal regulatory signals that would normally inhibit cell proliferation. This feature is usually linked to changes in tumor suppressor genes.

IV. Resistance to apoptosis, meaning that they can avoid the programmed cell death that normally occurs to remove damaged or old cells from the body to avoid error propagation, and therefore allows cancer cells to keep accumulating.

V. Sustained angiogenesis, or the formation of new blood vessels to supply the nutrients and oxygen needed for tumor growth. This process is linked to the expression of growth factors such as EGF, VEGF, and TGF-beta.[5,7]

VI. Metastasis, which involves the spread of cancer cells beyond their initial boundaries, invading neighboring tissues and ultimately affecting other parts of the body. This capability is facilitated by the tumor microenvironment, which supplies cancer cells with essential resources such as oxygen, nutrients, and structural support.

VII. Reprogramming of cellular energetics and metabolism, allowing cancer cells to grow and divide more rapidly due to the change in the way they use energy and nutrients and produce metabolites and biomolecules. This feature was proposed by Hanahan and Weinberg in 2011.

VIII. Evasion from immune response, through mechanisms such as altered presentation of antigens and production of immunosuppressive factors. Immune evasion was also added to the list of hallmarks in 2011.

The 2011 update also proposed that genome instability and tumor-promoting inflammation should be regarded as two enabling characteristics,[5] as their acquisition can contribute to the emergence of these features.

Additionally, in 2022, Hanahan suggested the incorporation of phenotypic plasticity and the existence of senescent cells as developing hallmarks.[6] Furthermore, he identified epigenetic reprogramming and polymorphic microbiomes as enabling factors that contribute to the initiation of this condition.

1.2 Metabolic rewiring in cancer: the Warburg effect and glutamine addiction

Metabolic rewiring, also known as metabolic reprogramming, is a defining characteristic of cancer that plays a crucial role in the development of the disease. This process involves altering cellular metabolism to adapt to nutrient-deprived and hypoxic conditions, enabling rapid proliferation and survival.

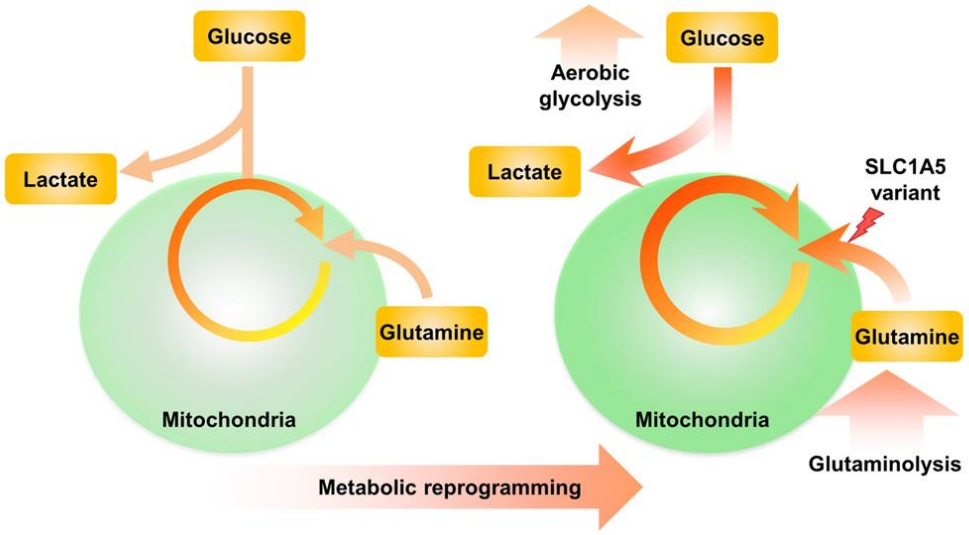

Figure 3 - Metabolic reprogramming relative to glucose and glutamine. In proliferative cells, aerobic glycolysis is linked to increased glucose uptake and secretion of most glucose-derived pyruvate as lactate, while glutaminolysis is boosted following higher glutamine import via the SLC1A5 variant transporter, thus supporting mitochondrial function through fueling of the TCA cycle.

Source: Adapted from YOO *et al*.[8]

Oncogenic activity (such as by *MYC, RAS, mTOR*, and *HIF*) contributes to these alterations alongside mutations in metabolic genes and extrinsic factors like nutrient availability. The effects of metabolic rewiring are not limited to energy metabolism but also extend into macromolecule biosynthesis and redox homeostasis, as well as gene expression involved in critical processes such as cell proliferation and angiogenesis influencing tumor microenvironment's immune response evasion mechanisms during differentiation stages.[9-12] Understanding and targeting specific metabolic mechanisms and vulnerabilities can provide insights and potentially lead to the development of more effective therapeutic strategies.

One aspect of metabolic reprogramming in cancer is the addiction to specific pathways such as the glycolytic and the glutaminolytic pathways. The Warburg

effect,[13-15] or aerobic glycolysis, is one of the main metabolic changes: unlike normal non-proliferative cells, cancer cells exhibit increased uptake of glucose and fermentation of glucose to lactate, a trace typical to hypoxia, even in the presence of oxygen.

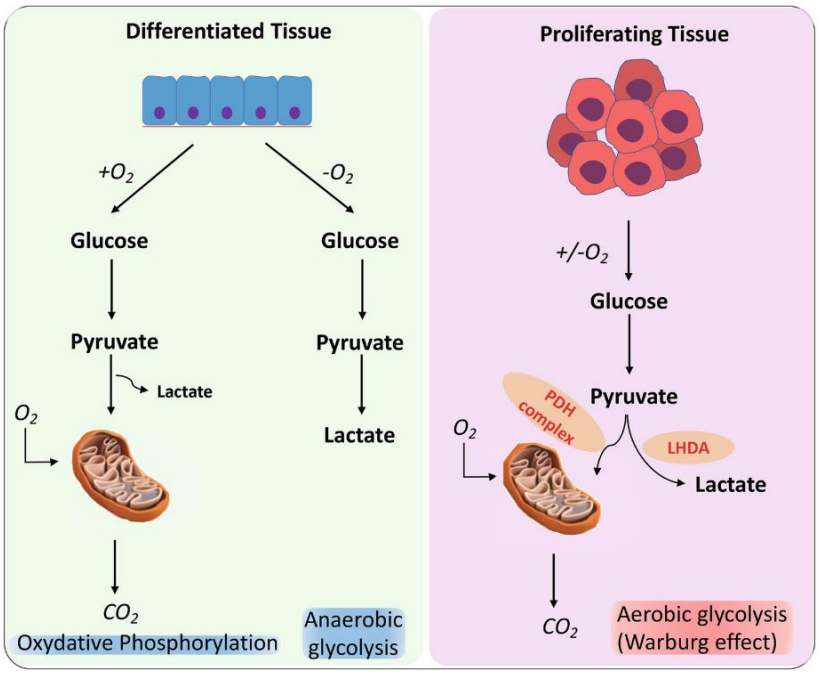

Figure 4 - Respiration in normal tissue (left) as opposed to aerobic glycolysis present in proliferating tissue (right).

Source: BOSE; ZHANG; LE.[16]

The Warburg effect is an inefficient means of ATP production compared to mitochondrial oxidative phosphorylation considering yield per glucose molecule. Warburg's initial hypothesis for this was that cellular respiration in tumor would be altered or damaged due to mitochondrial dysfunction; therefore, activation of the glycolytic pathway would provide advantages like macromolecule synthesis from metabolic intermediates. Several alternative explanations have been proposed so far, such as that it happens at a higher rate, so cells have a selective advantage in a limited resource environment, to support biosynthetic requirements for anabolic reactions, or to confer cells direct signaling functions.[15-18] However, the suppositions lead to pertinent counterpoints and questions, being a subject of controversy, and the intricacies of the causes and functions of aerobic glycolysis remain unclear. However, it is known that it involves changes in glucose transporters (GLUT), enzymes in the

glycolytic pathway, the hypoxia-inducible factor and monocarboxylate transporter, and is also influenced by genetic reprogramming, oncogenes like *KRAS* and *BRAF*, and tumor suppressor proteins like p53.[15-18]

Other than glucose, glutamine (Gln) is one of the most important nutrition sources for cancer cells – its catabolism provides them with carbon and nitrogen for biosynthetic reactions, fuels the TCA cycle, resulting in ATP production, plays a key role in antioxidative mechanisms, and has a part in regulation of intracellular signaling.[8-9,19-22] Its importance in cancer is becoming more widely recognized and has been receiving increasing attention for therapeutic approaches.

The most abundant amino acid in the blood, glutamine is transported into the cell via plasma membrane transporters such as SLC1A5, SLC38A1, and SLC38A2,[8,23] and into the mitochondrion through SLC1A5 variant.[24] Besides contributing to mechanisms such as the generation of important molecules for signaling, gene expression and cell metabolism, Gln undergoes the glutaminolytic pathway, starting by being converted into glutamate and ammonium by hydrolytic deamidation. The product is further oxidized into α-ketoglutarate by glutamate dehydrogenase (GDH), in a reaction where the cofactor $NAD(P)^+$ is reduced into NAD(P)H, and the main product is directed to fuel the TCA cycle. Therefore, the uncontrollable appetite of cancer cells for relevant versatile nutrients leads to the development of a “glutamine addiction,”[19-22] so that the amino acid participates in the anaplerotic process in the Krebs cycle, fulfilling biosynthetic needs.

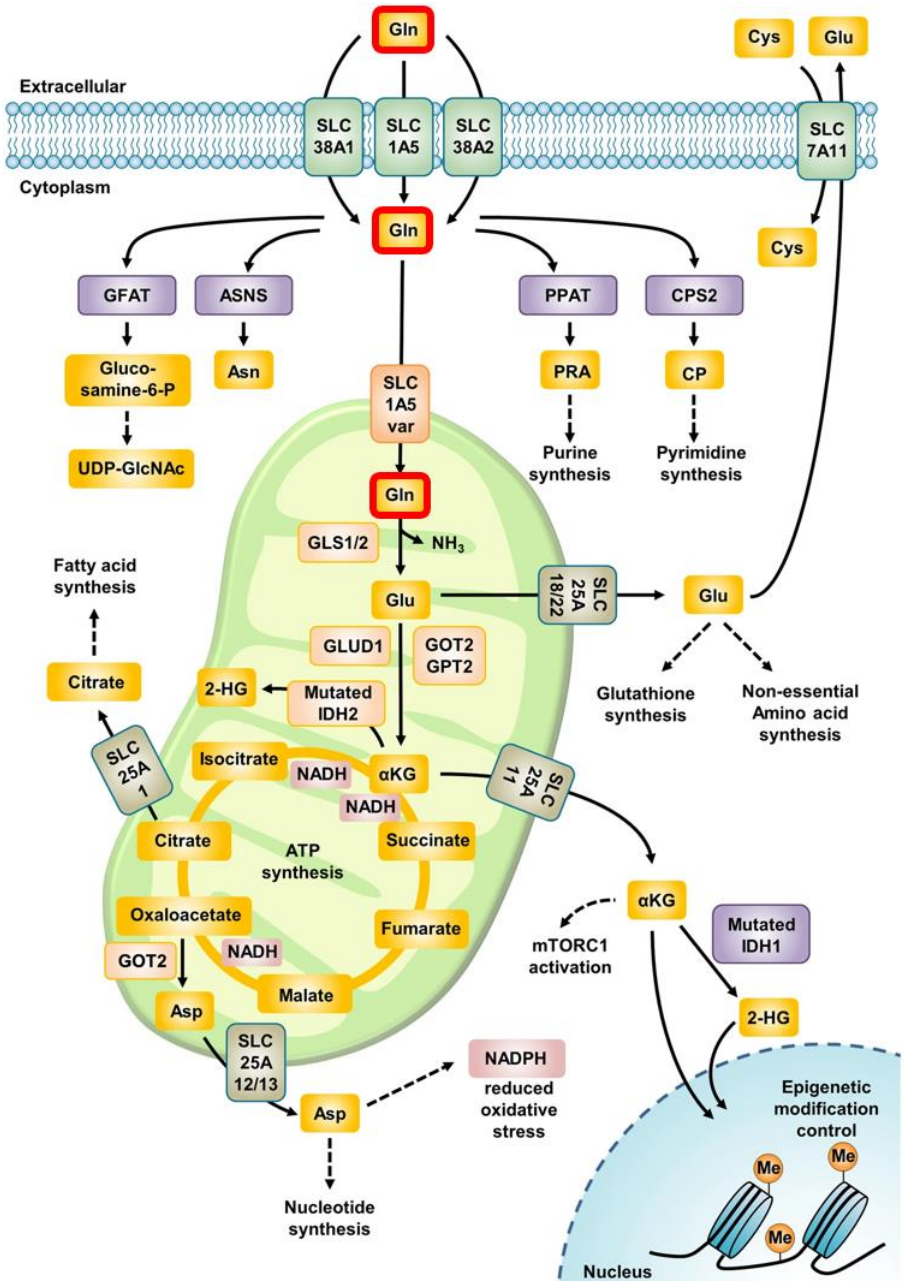

Figure 5 – Glutamine (Gln) metabolic pathways. Gln (boxes outlined in red) flux into the cell is given by transporters such as SLC1A5 and SLC38A1 prior to usage in mechanisms like biosynthesis of asparagine (Asn) and nucleotides. The SLC1A5 variant transporter is responsible for Gln import to the mitochondrion, where glutaminolysis (by glutaminase, producing glutamate) takes place. GLUD1, or GDH, catalyze the deamidation of glutamate into α-ketoglutarate (α-kg), supplying metabolites for the TCA cycle. Epigenetic remodeling can occur by 2-hydroxyglutarate (2-HG) and α-kg, which can also activate the mTORC1 pathway. Gln: glutamine; Glu: glutamate; Asn: asparagine; Cys: cystine; Asp: aspartate; αKG: α-ketoglutarate; GFAT: glutamine-fructose-6-phosphate transaminase; UDP-GlcNAc: Uridine-diphospho-N-acetylglucosamine; CPS: carbamoyl phosphate synthetase; PRA: 5-phosphoribosyl-1-amine; CP: carbamoyl phosphate; ASNS: asparagine synthetase; PPAT: phosphoribosyl pyrophosphate amidotransferase; GLS: glutaminase; GLUD: glutamate dehydrogenase; GOT: glutamic-oxaloacetic transaminase; IDH: isocitrate dehydrogenase; GPT: glutamic-pyruvate transaminase; 2-HG: 2-hydroxyglutarate; Me: methylation.

Source: Adapted from YOO *et al*.[8]

1.3 Glutaminases

Glutaminases[25] (EC 3.5.1.2) are the first enzymes in the glutaminolytic route, promoting the conversion of Gln to glutamate concurrently with the generation of an ammonium ion; therefore, they are among the key players in metabolic adaptation in tumors. It has also been linked to inflammation and neurological disorders, including neurodegenerative diseases such as multiple sclerosis and Alzheimer's disease.[26-28] Its medical importance has led to great interest in the development of glutaminase inhibitors like BPTES and CB-839.[29-32]

There are 4 Glutaminase isozymes known so far in mammals, products of two distinct genes located in different chromosomes.[33] *GLS* is in chromosome 2 (2q32.2) and spans 82 kb. It comprises 19 exons and codes for the glutaminase C (GAC) and kidney-type glutaminase (KGA), which are products of alternative splicing in the final portion of the gene, meaning that their C-terminal regions share only 12% sequence identity. It has also been reported to encode glutaminase M (GAM), a form that shows no measurable catalytic activity.[34] The GAC mRNA is formed by exons 1 to 15. KGA mRNA, on the other hand, is composed by the joining of exons 1-14 and 16-19, as indicated in Figure 6.[33,35]

GAC is usually expressed in the heart, pancreas, kidney, and lung,[33,36] and has also been detected later in the brain.[37] Elevated GAC mRNA levels have been reported in colorectal adenomas and carcinomas,[38] gliomas,[39] and breast tumors.[34] Meanwhile, KGA can be found primarily in the brain and kidney, as well as intestinal cells,[34,36] but not in the liver. The *MYC* oncogene has been shown to drive dysregulation of glutamine, glucose, and lipid metabolism in cancers, upregulating glutaminolysis and inducing high GAC expression in B lymphoma and prostate cancer.[40] Additionally, c-Jun activation also leads to increased GLS expression and glutaminase activity.[41]

The *GLS2* gene (12q13.3 on the human genome), on the other hand, has an approximate length of 18 kb, having 18 exons. GLS2 expression levels are regulated by p53 depending on stress conditions. Liver-type Glutaminase (LGA) and Glutaminase B (GAB, also called "LGA long" or "longer LGA" due to insufficient adoption of the "GAB" in the literature) are produced by using alternative promoters in *GLS2*. While the LGA transcript is made up by the joining of exons 2-18, the GAB transcript is composed of all the 18 exons.[33] LGA was originally described as present

in the liver,[42] but recent work has also demonstrated its existence in the brain,[43] pancreas, and in breast cancer cells.[36,44]

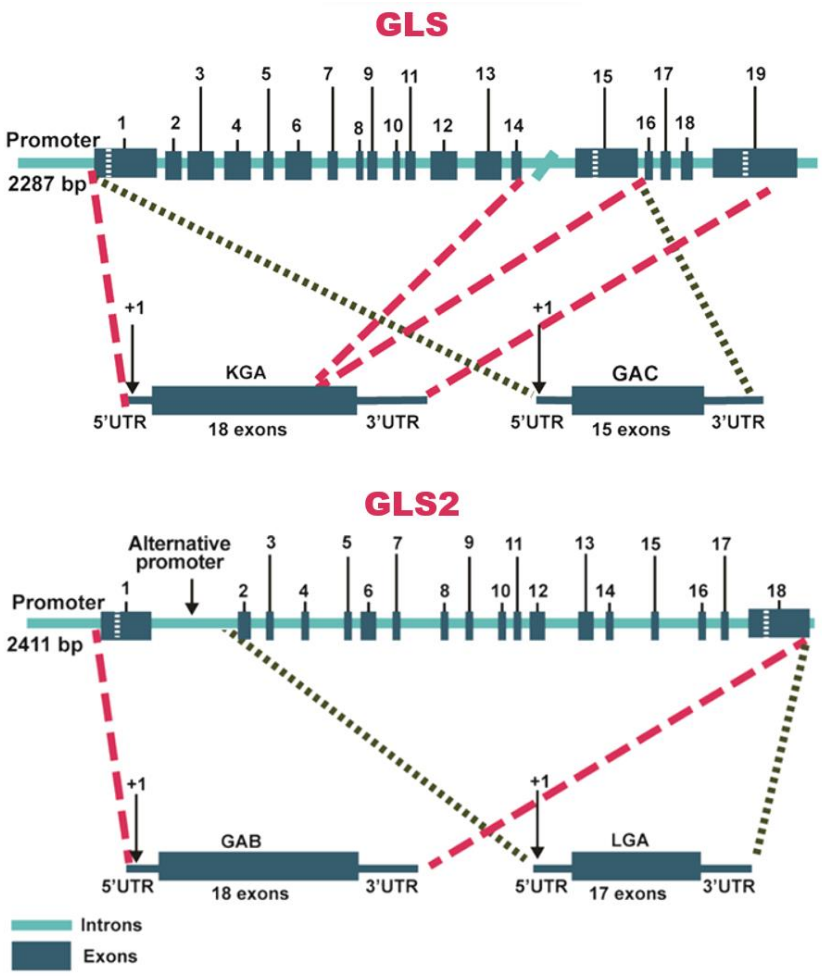

Figure 6 - Genes and mRNA transcripts of the glutaminase isozymes. At the top, GLS and alternative transcripts KGA and GAC. A third isoform, GAM, has also been reported previously. Bottom, GLS2 with GAB and LGA. Introns are represented by light blue lines and exons, by dark blue boxes.

Source: Adapted from CAMPOS-SANDOVAL *et al.*[35]

GLS is often associated with malignancy in cancer, being overexpressed in different cancer cell lines and tissues. Conversely, there is evidence that *GLS2* can act as either an oncogene or a tumor suppressor, depending on certain types of cancer.[45-46]

Although the mammalian genes *GLS* and *GLS2* are located in distinct chromosomes, they exhibit significant sequence similarity. It is speculated that *GLS*

and *GLS2* originated from a common ancestral gene, through gene duplication followed by gradual sequence changes leading to divergent evolution.[47]

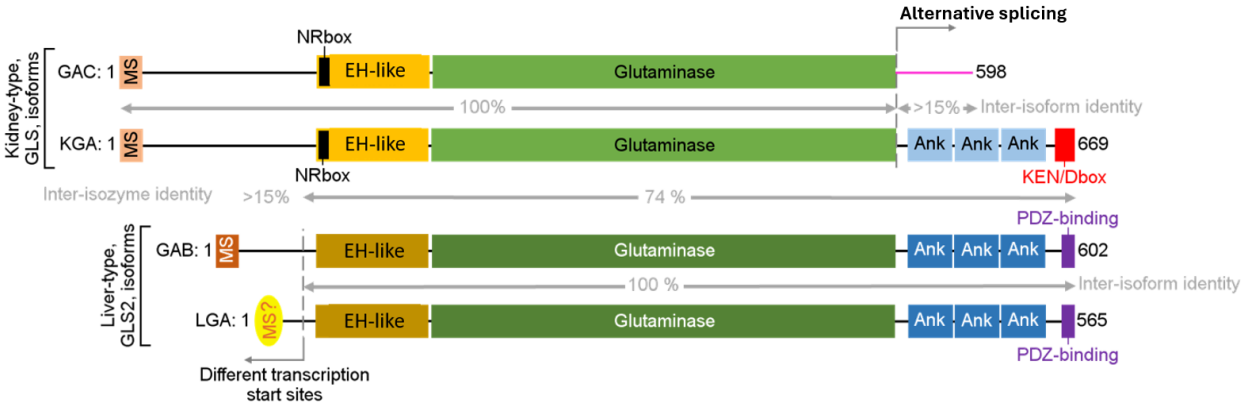

Figure 7 - Domain compositions of GLS and GLS2 isoforms. The glutaminase domain is well-conserved. The N-terminal domain is folded in an EF-hand-like four-helix bundle; while GAC has a truncated C-terminus, the other isozymes exhibit ANK repeats, followed by PDZ-binding motif in the GLS2 isoforms and a KEN/D box sequence in KGA.

Source: ADAMOSKI *et al.*[59]

Unlike KGA, GAC lacks the ankyrin (ANK) repeats present in KGA and GLS2 adjacent to the catalytic domain. The ANK domain is typically responsible for the mediation of protein-protein interactions, being reported with functions including regulation of cell cycle, ion transport, transcription and cell-cell signaling. KGA also possesses KEN box and D box sequences, known for interactions with ubiquitin ligase complexes that signal for protein degradation.[33]

The NR box motif sequence (LXXLL), commonly found in protein-protein contacts linked to regulation of nuclear receptors, is present in all glutaminase isoforms, at the N-terminal region. In fact, the presence of LGA has been observed in the nuclei of neuronal cells in the mammalian brain before.[33]

GLS2 contains a consensus sequence, equivalent to the amino acids ESMV at its C-terminal end, responsible for association with PDZ domain-containing proteins, after the ANK repeats. PDZ proteins can act as scaffolds interacting with short peptides for assembly of supramolecular complexes at specific cellular areas.[33]

Additionally, both *GLS*-derived isoforms, as well as GAB, exhibit the signal sequence for mitochondrial localization, while it is still unclear whether the same

happens in LGA. However, the only isozyme shown to be exclusively present in the mitochondria is glutaminase C.[33]

The N-terminal region presents a domain folded in an EF-hand-like manner.[47] Usually, the loop in the EF-hand domain presents areas for Ca^{2+} binding and is present in proteins like the signaling protein calmodulin and the muscle protein troponin-C. These can often undergo a calcium-dependent conformational change, creating a site that enables their binding to a target.[48-50] Nevertheless, there has been no substantial evidence of functional activity for this region in glutaminases to this date.

1.4 Glutaminase C (GAC)

Particularly, several tumor cell lines have presented high GAC mRNA levels, and upregulation of GAC expression was found to be essential for cell proliferation and survival in cancer. Moreover, a study conducted in 2010 by J.B. Wang and colleagues[29] investigated an inhibitor reported to block oncogenic transformation induced by Rho GTPases that was revealed to target GAC. The available body of evidence served as motivation for research with focus on the structural and biochemical properties of GAC, aiming to comprehend the molecular basis of its activity and distinguish it from KGA, LGA and GAB, published in 2012 by our group and partners.[51]

Immunohistochemical analyses revealed that both KGA and GAC expression levels were increased in breast cancer, with a positive correlation with tumor grade. However, immunoblotting with isoform-specific antibodies showed that GAC was the only isozyme with an exclusive mitochondrial locale for lung, breast, and prostate tumor cell lines, as stated previously.

Further investigation pointed to GAC as the most efficient isozyme upon addition of phosphate, a trace that becomes accentuated the higher the Pi concentrations tested.[32] This property is especially interesting, considering that phosphate levels are higher in tumor cells in hypoxic situations.[52-53] Therefore, it contributes to the hypothesis that GAC would be the key glutaminase isozyme in tumors.

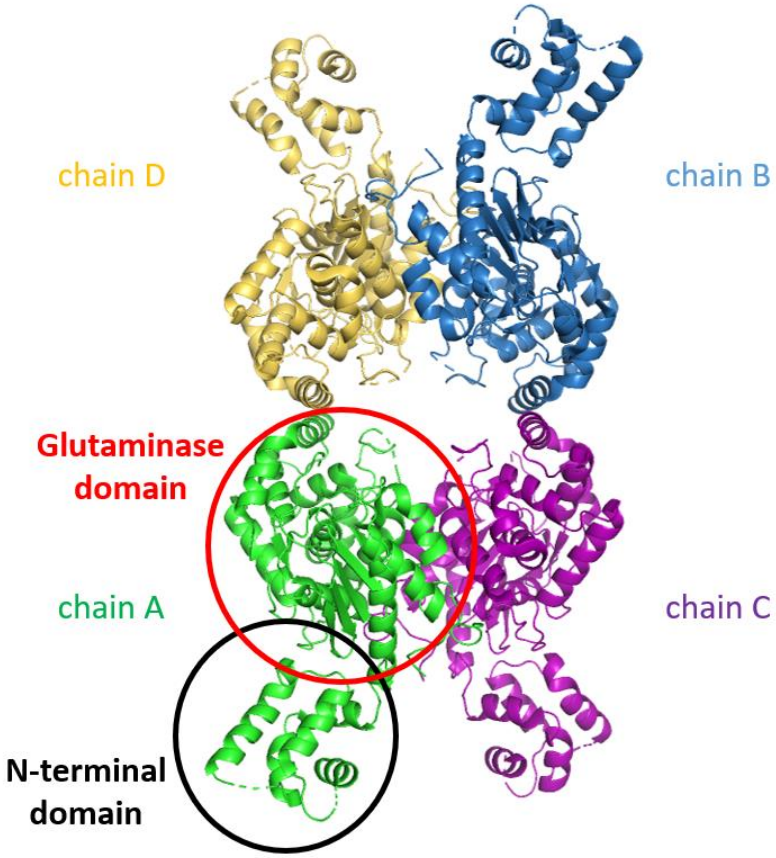

Figure 8 - Crystal structure of GAC (PDB 3ss3). Circles in chain A show both the glutaminase and the N-terminal domains. Despite representation, the C-terminus possesses a heterogeneous conformation and could not be successfully modeled.

Source: By the author.

GAC structure (PDB 3ss3), elucidated by X-ray crystallography[51] and shown here in Figure 8, reveals the tetramer as a dimer of dimers (formed by chains A and C and chains B and D). In the N-terminal region, the residues L144-N221 fold into the EF-hand-like four-helix bundle structure. Among these, L144-L148 form the NR box motif. The glutaminase domain, from the β-lactamase/transpeptidase-like superfamily, consists of residues K249-Y535. Its active site is located between a subdomain composed purely of α-helices and an α/β/α sandwich subdomain. It is highly cationic and contains all the contacts that define formation of both the dimers (the dimeric interface is formed by 45 residues from each monomer) and the tetramers. The oligomer is characterized by a relative twist of about 25° between dimers along its shortest axis, and its interface is defined by the stacking of equivalent α-helices (D391-K401). The opposite charges of the residues placed in the ends of each helix allow for proper orientation of the interaction pair.

A region called the gating loop, or activation loop, is comprised of residues L321-F327 (L321-RFNKL-F327, NCBI reference sequence NP_001106854.1), near the catalytic site, and is important for the regulation of active site accessibility – upon tetramerization (dependent on concentration), the loop adopts an open state which leads to higher protein affinity for the substrate. Another area, called the lid loop, is formed by residues V251-D264, and contains a YIP motif suggested as an additional feature that closes off the active site after substrate binding.

The enzyme is inhibited by the product of the reaction. However, phosphate competes with glutamate for the same interactions in the cationic catalytic site, liberating glutaminase from inhibition, thereby guaranteeing the enzyme cycling. Therefore, Pi stabilizes tetramers in a more active state, increasing turnover rates.

In 2013, a piece published by our group shed some light on molecular mechanisms of phosphate-dependent glutaminase activation.[32] We investigated the assembly of GAC superstructures and its relationship with enzymatic activation *in vitro* and in human breast cancer cell model. The fiber-like oligomers, or filaments, presented a tendency that correlated positively with activation levels produced by Pi. KGA and GLS2 proteins were also tested, showing that KGA forms shorter filaments, whereas GLS2 presents no oligomerization of higher order. In addition, the GLS inhibitor BPTES hindered polymerization through the stabilization of inactive tetramers.

Key residues were found to be involved in the filamentation process: mutation of R322A impaired activation and polymerization; the mutant K316Q (which explored a post-translational modification of human GLS, the lysine acetylation) also lacked higher order oligomerization; and the gating loop mutant K325A exhibited superstructure formation and a 600-fold increase in catalytic efficiency, even without inorganic phosphate. K325A in MDA-MB 231 cells manifested enhanced proliferation and uptake of glutamine in comparison to the control groups. Furthermore, the work disclosed a novel low-resolution model for the superstructure, based on a double-stranded helix where each strand was formed by end-to-end interactions of the N-termini domain of GAC tetramers.

In a later paper from 2017,[47] the structures we discussed for KGA and GLS2 collaborated in the question of why these cannot form as active supra-tetrameric filaments as is the case with the C-terminally truncated GAC. It was suggested that the presence of the bulky ANK repeats might be essential to adjust catalytic activity and disadvantage filamentation in KGA/GLS2, by establishing intramolecular interactions

to form ANK dimers that lead to the obstruction of a groove region deemed necessary for tetramer association into higher-order oligomers.

Further information on the exact molecular mechanism of GAC activation and filamentation induced by Pi is not fully comprehended yet. Therefore, our purpose is to provide deeper insight into the process leading to GAC polymerization and activation.

2 OBJECTIVES

2.1 General Objective

The goal of this project was to investigate the interaction mechanism in the enzyme Glutaminase C as revealed by single-particle cryo-EM through site-directed mutagenesis in the filament interface and activation loop, seeking to verify how they influence GAC higher-order oligomerization and super-activation, and consequently validating a new reliable model for the glutaminase filament.

2.2 Specific Objectives

1. Construction of GAC mutants based on the tetrameric interaction interface and the activation loop residues (F323S, L326S, F378S, F383S, R387D, K325A/L326S), aiming to identify key residues in GAC filamentation and activity.
2. Expression of recombinant proteins in *E. coli* Rosetta 2 cells.
3. Purify GAC in three steps – affinity, ion exchange, and size exclusion chromatographic methods.
4. Evaluate possible changes in oligomeric state resulting from point mutations upon phosphate addition by dynamic light scattering.
5. Biochemical characterization of wild type and mutant GAC activity in the absence or presence of inorganic phosphate by a GDH-coupled kinetic assay measuring NADH production by absorbance at 340 nm.
6. Adjust analyzed data to a structure of the GAC filament obtained by cryogenic electron microscopy (cryo-EM).

3 MATERIALS AND METHODS

Because of the high similarity of the glutaminase domain between the mouse (mGAC) and human (hGAC) GAC sequences, all experiments were carried out with mGAC. The difference is in the position number of residues so that position n for human GAC corresponds to to n+5 in the mouse sequence.

3.1 Site-directed mutagenesis and cloning

Our aim was to establish the determinants of GAC activation and filamentation upon Pi binding. Therefore, after careful analysis of available ligand-free and substrate-bound GAC structures on PDB, site-directed mutations were planned in residues of the activation loop, previously shown as important to oligomerization and activity, as well as in a region thought to participate in the interaction interface between tetramers. Additionally, a double mutant combining the gain-of-function, filamentation-inducing K325A and the adjacent residue L326S (which, contrarily, impaired tetrameric change) was tested.

Table 1 - Oligonucleotides (F) utilized in the GAC constructs.

Oligonucleotides	Sequence
mGAC F323S F	TGGATTAAGAAGCAACAAACTCTTTTTG
mGAC L326S F	GTGGTTTATCATCTTCATTCAAAAAGCTTTTGTTGAATCTTAATCCACTTGGCT
mGAC F378S F	AGACTGAAACGTTGCATTACTGCTTCCAACATATTCATTACCAGCC
mGAC F383S F	CCACTTTCTCGTTCAGACTGACTCGTTGCATTACTGAATCCAAC
mGAC R387D F	TTGCAAAATTTCGATCTCCACTTTCATCTTCAGACTGAAACGTTGCATTACTG
mGAC K325A/L326S F	GCCAAGTGGATTAAGATTCAACGCAAGCTTTTTGAATGAAGATGATAAACCA

Source: By the author.

Mutagenesis with the QuickChange Site-Directed Mutagenesis kit (Agilent) was performed in collaboration with our colleagues at LNBio (CNPEM) in mGAC CDS (NM_001113383.1) Δ128-603, cloned in pET-28a vector (Merck Millipore) with the primers listed on Table 1.

3.2 Heterologous expression

Wild-type and mutant GAC plasmids (pET-28a, Δ128-603) were transformed in *E. coli* cells from the DH5α strain (Merck Millipore) by heat shock for propagation and stock of the mentioned constructs. For heterologous expression of the recombinant proteins, heat shock transformation was performed in chemically competent Rosetta 2 *E. coli* cells (Merck Millipore).

After completing small-scale expression tests (by addition of 1 mM IPTG for induction for 3 hours at 37 °C in LB medium), the transformants were grown from a single colony picked from agar plates. Cells grew overnight in LB medium with the appropriate selective antibiotics – 50 µg/mL kanamycin and 50 µg/mL chloramphenicol – at 200 rpm, 37 °C. The following day, 10 mL of the culture were added to 1 L of LB medium and grown in the same conditions for approximately 5 hours, until OD_{600} reached between 0.6-0.8. Temperature was lowered to 18 °C and the expression was induced with 0.2 mM IPTG for 18 hours, with agitation at 200 rpm.

Finally, cells were centrifuged at 4 °C, 4000 rpm for 40 minutes and pellets were flash-frozen in liquid nitrogen for storage at -80 °C.

3.3 Purification

The recombinant proteins were purified in three subsequential steps of different categories of chromatography, exploring distinct physicochemical properties.

Firstly, cells were thawed and resuspended in the resuspension solution, according to table 2. Lysis was done by incubating the samples for 1 hour, on ice, with the addition of 120 mg lysozyme, 60 mg DOC (deoxycholic acid) and 100U benzonase per culture liter.

Next, samples were centrifuged at 12 000 rpm, 4 °C, for 1 h 20 min for collection of the soluble fraction, and the supernatant was used for the first chromatography step.

Table 2 - mGAC resuspension and purification buffer compositions.

Buffer	Composition
Resuspension	50 mM Tris pH 8.5, 500 mM NaCl, 10% glycerol, 2 mM β-mercaptoethanol, and 2 mM PMSF
Affinity	50 mM Tris pH 8.5, 2 mM β-mercaptoethanol, and 10 mM NaCl
A, ion exchange chromatography	50 mM Tris pH, 10 mM NaCl and 2 mM DTT
B, ion exchange chromatography	50 mM Tris pH, 1 M NaCl and 2 mM DTT
GF, size exclusion chromatography	30 mM Tris pH 8.5, 150 mM NaCl and 0.5 mM TCEP

Source: By the author.

3.3.1 Affinity chromatography

For immobilized metal affinity chromatography (IMAC), 1.5 mL of the Co^{2+}-charged TALON® Superflow resin (Clontech) was used per liter of culture. The column was washed and equilibrated previously with affinity buffer (table 2), to hamper promiscuous interactions within the column.

After the soluble fraction of the cellular extract was loaded onto the resin, the flow-through was collected prior to washing of the column with the affinity buffer. Subsequential washing steps were carried out with different imidazole concentrations (5 mM and 20 mM) to wash away possible contaminants.

The proteins were then eluted with 250 mM imidazole in the affinity solution. Samples were incubated with 60 U thrombin (Sigma Aldrich) for overnight removal of the C-terminal His-tag.

3.3.2 Ion exchange chromatography (IEC)

Ion exchange chromatography, which separates proteins based on their net electric charge, was performed on an ÄKTA pure™ FPLC system (GE Healthcare), by loading the proteins onto a HiTrap Q FF (anion exchange, positively charged) column (GE Healthcare) after equilibration with buffer A (table 2).

Ion exchange was performed at a flux of 1 mL/min. Column was washed with increasing gradient of buffer B (from 10 mM to 1 M NaCl concentration), generated by the ÄKTA system, for protein elution. The eluate was concentrated at 4 °C in Amicon® centrifugal filters with a 50 kDa pore cut-off.

3.3.3 Size exclusion chromatography (SEC)

Following IEC, the samples were injected into an analytical Superdex 200 10/300 GL column (GE Healthcare) previously equilibrated with the GF buffer (table 2) for size exclusion chromatography with the ÄKTA FPLC system, separating sample components by molecular weight. SEC was performed with GF buffer (table 2) at a 0.5 mL/min flow rate. Protein concentration was measured by absorbance at 280 nm using the appropriate calculated extinction coefficient, and samples were analyzed on 12.5% SDS-PAGE.

3.4 Dynamic Light Scattering, DLS

Proteins were kept at a concentration of 1.5-3.0 mg/mL in buffer GF and tested after incubation for 1 hour with varying concentrations of K_2HPO_4, source for the inorganic phosphate (Pi) (0 and 20 mM; 100 mM for one of the mutants). To verify the capacity of NaCl to disrupt polymerization, increasing concentrations of NaCl were also tested in the wild-type enzyme (10, 200, and 500 mM).

Prior to application into a quartz cuvette, all samples were centrifuged at 10 000 g, 4 °C for 30 seconds to remove impurity aggregates. After a wait time of 5 minutes for equilibration in a ZetaSizer μV device (Malvern Panalytical Instruments), DLS measurements were taken in triplicate, at 25 °C. The size distribution was established in the Malvern ZetaSizer software. The results were plotted in GraphPad Prism v.8.0.

3.5 Enzymatic activity assay

Glutamate, the product of the glutaminase reaction, does not show absorbance in the UV visible light spectrum. Therefore, activity was measured indirectly in a coupled assay, where kinetic parameters of wild-type and mutant GAC were determined according to the procedure described by Cassago *et al.* (2012). Glutamate

is converted into α-ketoglutarate by GDH (glutamate dehydrogenase), a process that reduces NAD+ into NADH. For every glutamate molecule undergoing deamination, one NAD+ molecule is reduced; therefore, stoichiometry of the reaction is 1:1 and the velocity of GAC reaction can be gauged by NADH production at 340 nm instead.

The assay mix was prepared for every construct with 50 mM Tris-acetate pH 8.6, 0.2 mM EDTA, 2 mM NAD+, 0.6 U GDH (Sigma Aldrich), 10 nM mGAC, and different concentrations of K_2HPO_4 (0 mM and 20 mM). 80 µL of this mixture were added to 120 µL of serially diluted L-glutamine (at 60, 30, 15, 7.5, 3.8, and 1.9 mM final concentrations) in a flat-bottom 96-well plate. Total volume of the reaction was 200 µL.

In agreement with the DLS experiments, wild-type mGAC activity was also tested with NaCl at 10, 200, and 500 mM.

All assays were performed in triplicates, and NADH production was measured by absorbance at the 340 nm wavelength for 120 seconds at room temperature using the SpectraMax Plus 384 microplate reader (Molecular Devices). The initial velocities in picomoles/s were calculated using an extinction coefficient for NADH of 6 220 M^{-1} cm^{-1} at 340 nm and 0.5 cm of path length. Kinetic parameters were analyzed with the GraphPad Prism v8.0 software (GraphPad).

3.6 GAC Single-particle cryo-EM

Cryo-EM experiment was performed with our collaborators. Wild-type GAC was diluted to 0.3 mg/mL prior to incubation with 20 mM Pi (from K_2HPO_4) for 1 hour. The sample (2.5 µL) was applied on a Quantifoil R2/2 200 mesh copper grid treated with glow discharge. Grid preparation and vitrification were executed in a Vitrobot Mark IV (Thermo Fisher Scientific) at 4 °C with 100% humidity, 4.5 s blot time and -4 blot force. After blotting, a drain time of 0.5 s was applied before rapidly plunging the grid into liquid ethane.

Data collection was carried out on the 300 kV Titan Krios G3i (Thermo Fisher Scientific) microscope with a Falcon 3EC direct electron detector (Thermo Fisher Scientific) available at the LNNano Electron Microscopy Facility (CNPEM). The EPU software was used for automated data collection.

12566 movies were collected, with 20 fractions per movie, in 54.2 s, under a dose of 1.5 $e^-/Å^2$ per fraction (6 30 $e^-/Å^2$ total dose) in electron counting mode, in the

absence of a phase plate. Magnification was 59 000 x, pixel size was 1.1 Å and defocus was between -2.0 and -3.0 µm.

Data processing was executed by the supervisor of this project, Prof. Dr. Andre L. B. Ambrosio. After the movies were corrected for camera artifacts and anisotropic magnification distortion on the IMAGIC software, cryoSPARC was used for micrograph refinement (motion correction, fraction summation, and CTF estimation), particle identification, 2D classification, and extraction, *ab initio* reconstruction and refinement (nonuniform, helical, and local) for 3D map reconstruction.

4 RESULTS

Analysis of the available structural information of single-particle GAC structure, compared to early crystallographic structures, was useful in the design of mutations to study enzyme oligomerization and activation. On the activation loop, we constructed mGAC.F323S, mGAC.L326S, and mGAC.K325A/L326S. The latter combined two substitutions of opposing effects, based on the L326S construct that impaired polymerization (data shown in the following subsections) and the hyper-active K325A, which forms higher-order oligomers, as reported in the literature. Furthermore, mGAC.F378S, mGAC.F383S, and mGAC.R387D target the supposed interaction interface between GAC tetramers.

4.1 Heterologous expression

A small-scale expression test, with induction by 1 mM IPTG for approximately 3 hours at 37 ºC, showed that the native GAC and the GLS constructs were produced in soluble form in the *E. coli* cells from the Rosetta 2 strain. Protein expression was confirmed by 12.5% SDS-PAGE analysis of the soluble fractions, as indicated by Figure 9 below.

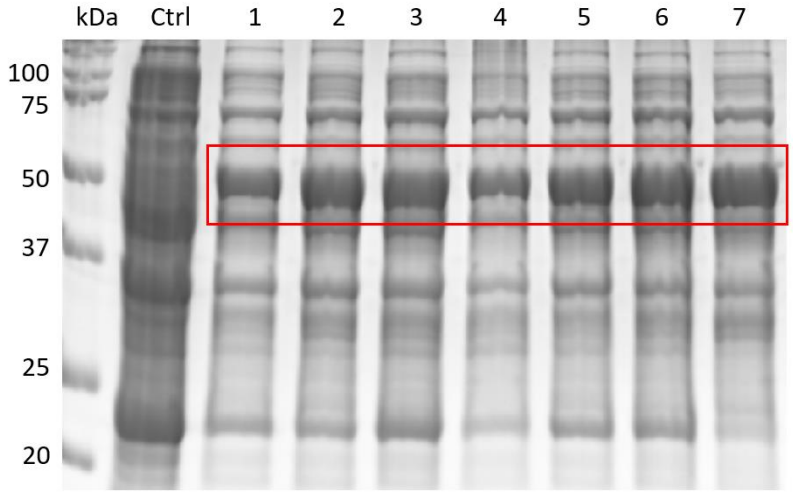

Figure 9 - mGAC expression test. The wild-type and mutant mGAC constructs (~ 50 kDa) were expressed in soluble form in Rosetta 2 E. coli cells and extracts were analyzed in 12.5% SDS-PAGE. Lane order is as follows: kDa – molecular weight marker (Precision Plus Protein Standards, Bio-Rad); Ctrl – WT mGAC, 0 mM IPTG; 1 – WT mGAC, IPTG-induced; 2 – F323S, IPTG-induced; 3 – L326S, IPTG-induced; 4 – K325A/L326S, IPTG-induced; 5 – F378S, IPTG-induced; 6 – F383S, IPTG-induced; 7 – R387D, IPTG-induced.

Source: By the author.

4.2 Protein purification

Following expression, cells were lysed, and protein purification was performed by affinity, ion exchange and size exclusion filtration chromatography protocols, respectively, yielding proteins with high level of purity. Afterwards, fractions went through confirmation by SDS-PAGE (12.5% gel). Figure 10 below shows the chromatogram profiles and SDS-PAGE for this step.

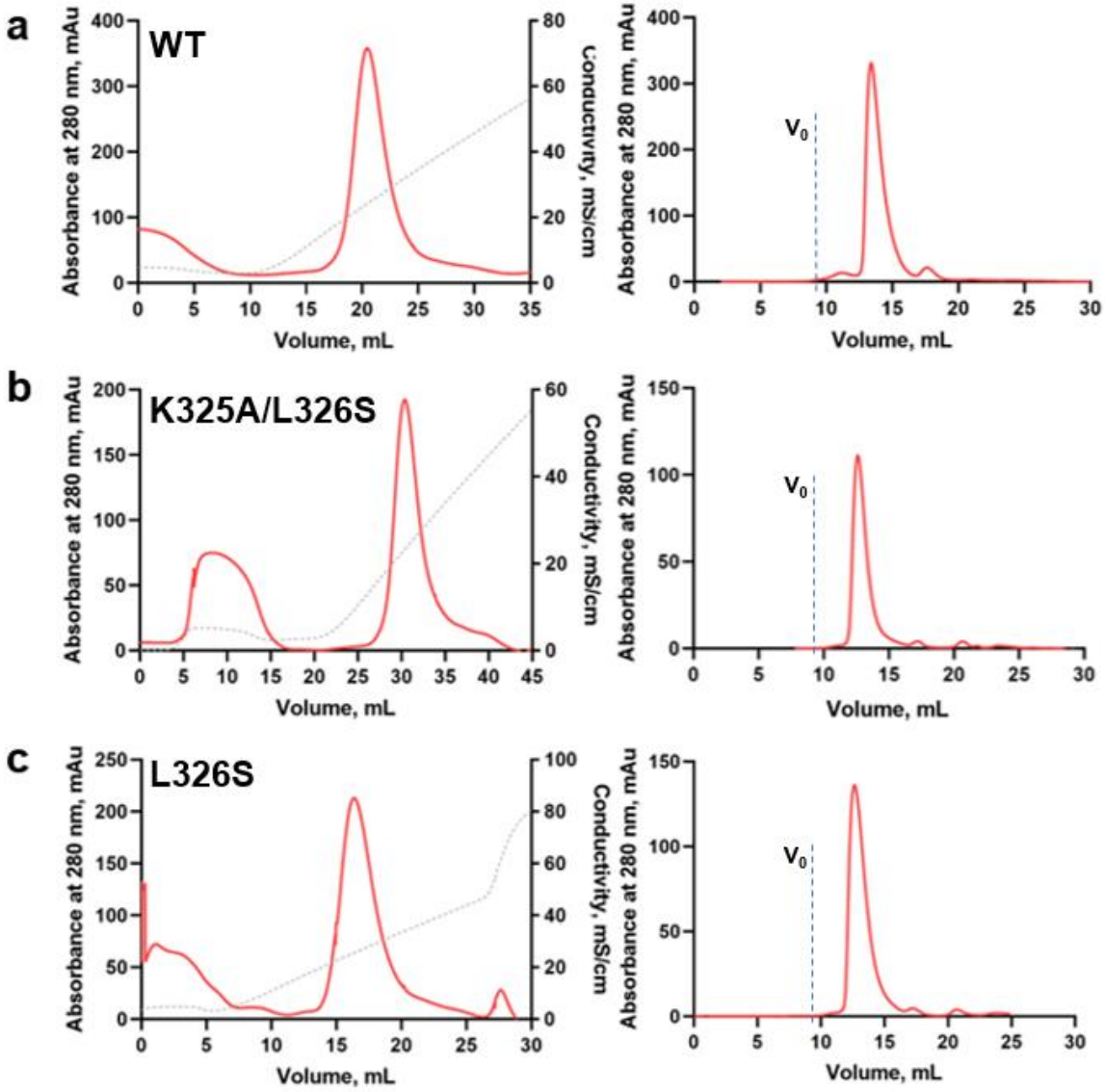

(continua)

(continuação)

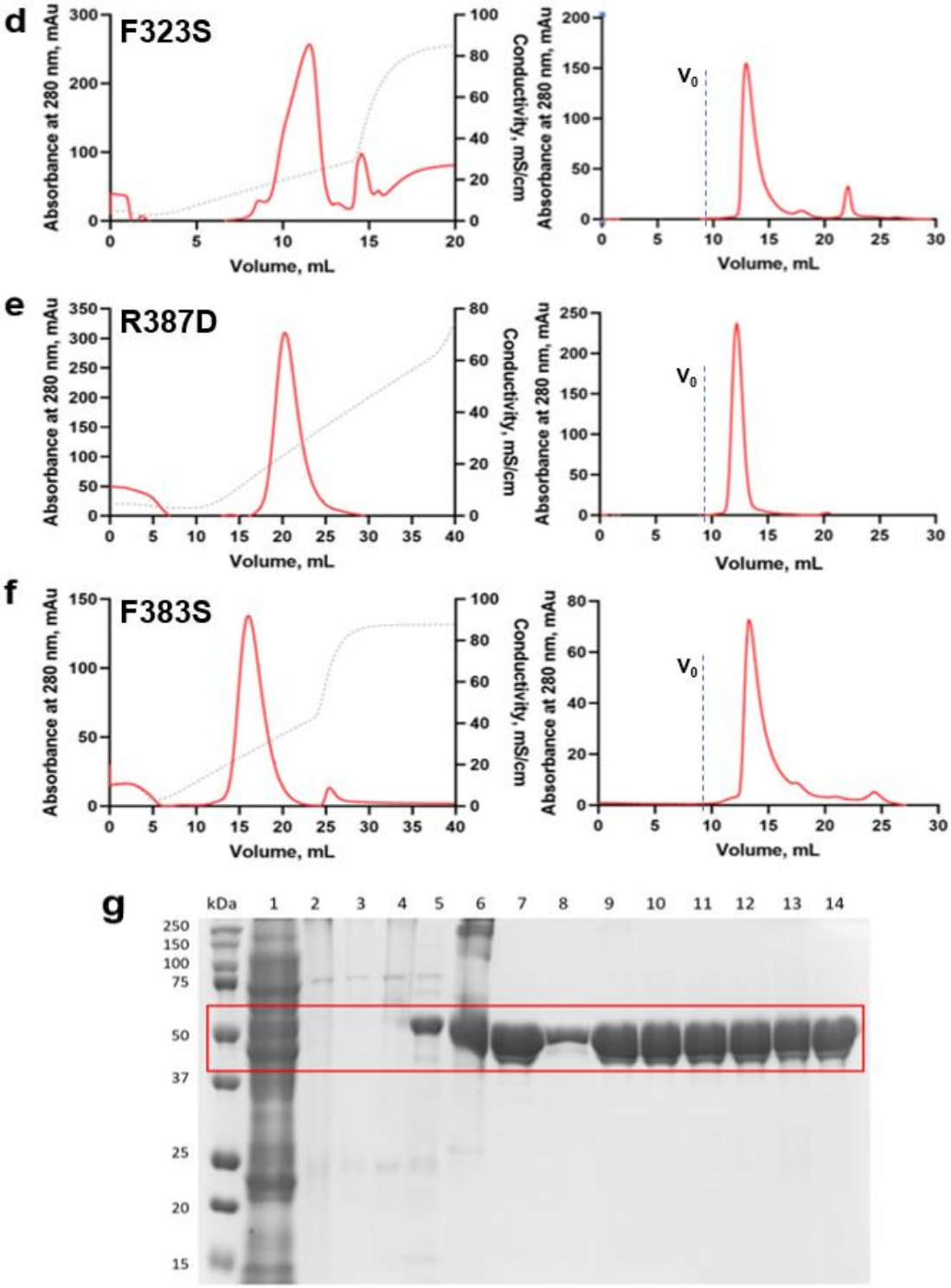

Figure 10 - GAC purification. Chromatographic profiles of IEC (left) and SEC (right) for GAC a) WT, b) K325A/L326S, c) L326S, d) F323S, e) R387D, and f) F383S. In g), 1 – the cellular extract, the steps of WT GAC affinity chromatography (2-5: wash steps, 6: affinity eluate), followed by WT GAC after purification by IEC (7) and SEC (8). Next lanes are post-SEC fractions from 9 – F323S, 10 – L326S, 11 – K325A/L326S, 12 – F378S, 13 – F383S, 14 – R387D, with concentrated proteins. V_0: column void volume.

Source: By the author.

4.3 Dynamic Light Scattering (DLS)

DLS measures fluctuations in the intensity of light scattered by a sample under a determined angle, caused by the Brownian motion of particles in solution. These fluctuations can be used to determine the diffusion coefficients and hydrodynamic radii of particles, which can lead to information about size distributions and sample homogeneity. Thus, the technique allows for confirmation of the oligomeric state in which GAC under each condition is found.

The resulting curves, expressing the size distribution as a function of hydrodynamic radii by volume, are shown for the constructs in the absence and presence of 20 mM Pi. Data for wild-type GAC (WT) is represented in red; a second control group (mGAC.K325A) was also evaluated and is shown in green in Figure 11. WT exhibits peaks in both the area around 6 nm radius (expected for the tetramer) and the filament region, showing heterogeneous species, while K325A presents a shift towards the higher-order oligomers in both conditions, as we anticipated.

The remaining graphs, corresponding to the planned mutations, are compatible exclusively with the tetrameric form for all proteins, lacking peaks in the filament size range, independent of phosphate concentration in the samples.

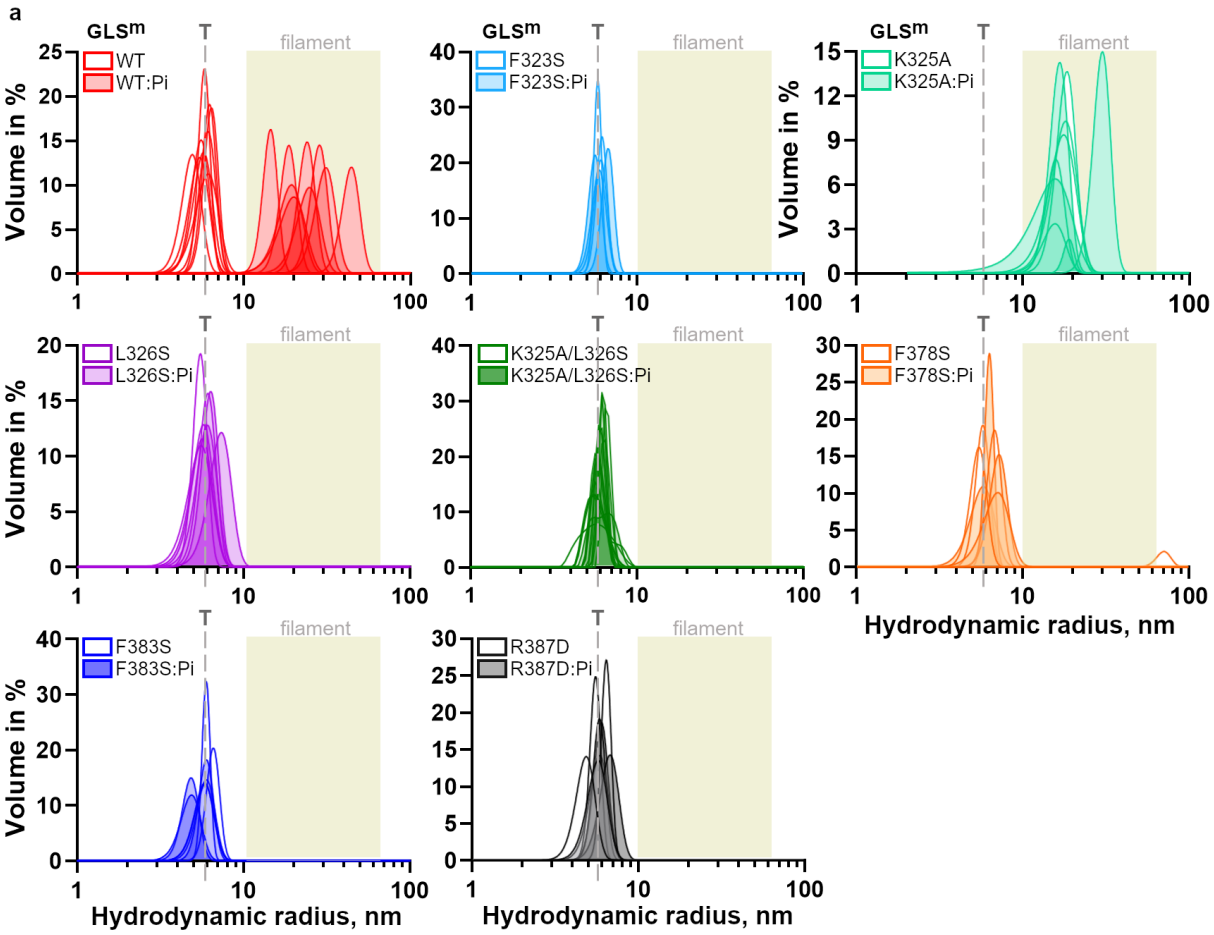

Figure 11 - DLS curves for GAC. The curves express size distribution as a function of the hydrodynamic radius by volume for mGAC (WT and point mutants). Empty and filled peak tracings represent the absence and presence of 20 mM Pi, respectively. A vertical dashed line (T) shows the expected radius for the tetramer, while the filaments are in the area colored in light yellow.

Source: Adapted from ADAMOSKI *et al.*[59]

To investigate the possibility to regain some of the polymeric state with a greater amount of phosphate, one of the mutants, R387D, was chosen for a new DLS test after incubation with 100 mM Pi. However, we observed that increasing phosphate availability did not promote filamentation (Figure 12).

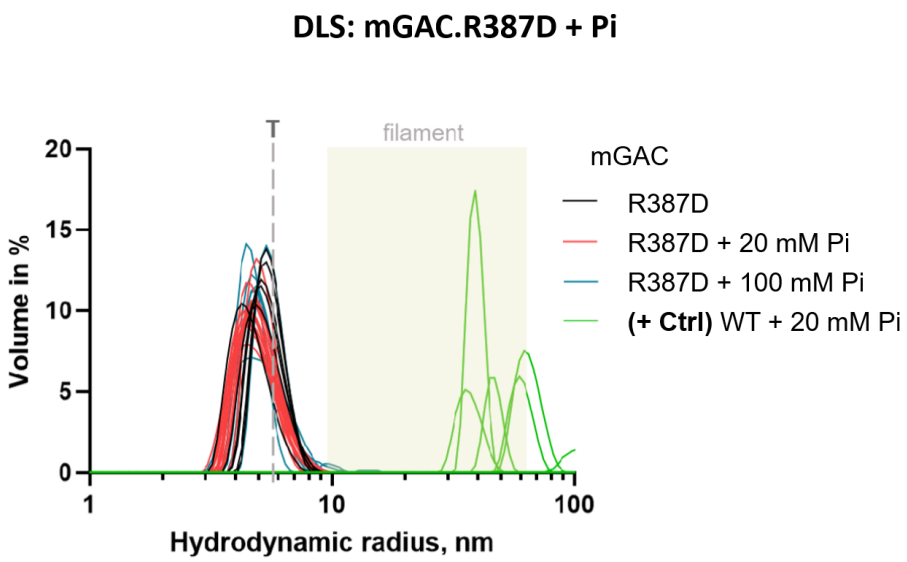

Figure 12 - DLS curves for mGAC.R387D, tetrameric mutant, with increasing phosphate concentrations.

Source: By the author.

Additionally, we verified the capacity of NaCl to interfere with filament or tetrameric assembly. DLS was performed in the WT enzyme incubated with 20 mM Pi, together with NaCl at 0.01, 0.2, or 0.5 M. The curves obtained for said circumstances are represented in Figure 13 below.

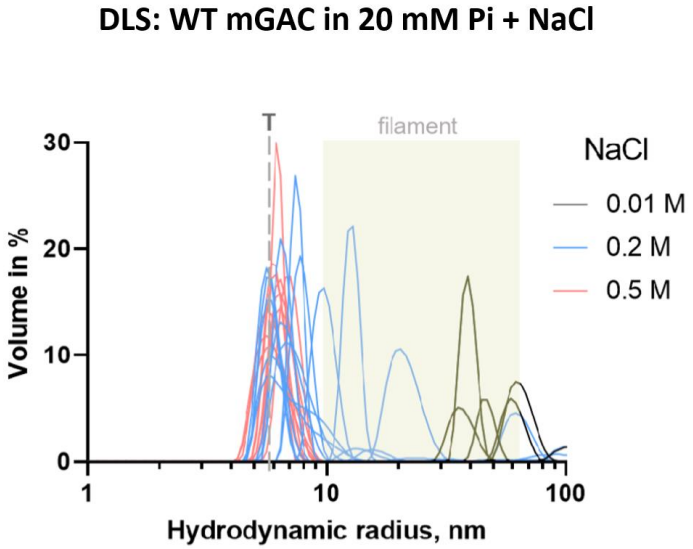

Figure 13 - DLS curves for WT mGAC with increasing concentrations of NaCl.

Source: By the author.

Our data show that the lowest amount of NaCl did not disrupt filamentation, with curves above the 20 nm radii range. It can be observed, nonetheless, that increasing concentrations of salt shifted the peaks to the left, leading up to solely the tetrameric form at the highest NaCl amount tested. This result agrees with the fact that mammalian kidney-type glutaminase structures were solved with high concentrations of salt in crystallization conditions (as seen, for instance, in PDB 5UQE, 5D3O, 5JYO, 5JYP, and 3VP0).

4.4 GAC activity assay

Enzymatic activities of WT and point mutants of mGAC were assessed indirectly as described in the Materials and Methods section (3.5), by a coupled assay with GDH and the detection of NADH production by UV absorbance at 340 nm, aiming to identify if any of the constructs would be stimulated upon the presence of phosphate, and correlate activity with oligomeric state of the proteins.

It is known that GAC traditionally obeys Michaelian kinetics with respect to glutamine. The Michaelis-Menten curves for all constructs are exposed in Figure 14. The mGAC.K325A construct was evaluated without Pi addition, due to its known spontaneous hyper-activation.

Mutations in the residues F323S, L326, R387, and K325/L326 decreased catalysis by more than half in comparison to wild-type GAC, while the interface targets F378 and F383 presented slightly higher velocities. This observation indicates that disruption of interactions with the designated residues is critical to the destabilization of glutamine hydrolysis by GAC. The association of these mutations with activity is further discussed in the structural analysis (subsection 4.5).

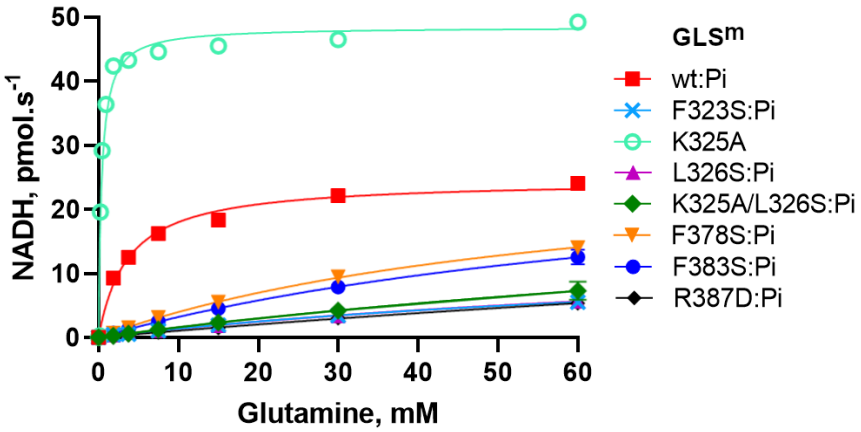

Figure 14 - Michaelis-Menten curves for all GAC constructs. Enzyme reactions were assessed indirectly through the GDH-coupled assay with 1:1 stoichiometric balance. mGAC.K325A activity was measured without the addition of 20 mM Pi.

Source: Adapted from ADAMOSKI *et al.* [59]

Characterization of kinetic parameters is shown in Figure 15; catalytic efficiency is given by k_{cat}/K_m. As expected, the wild-type enzyme is the second most efficient, following the K325A mutation, which shows an 18-fold increase. The loop and interface mutants display the lowest values when added of 20 mM Pi.

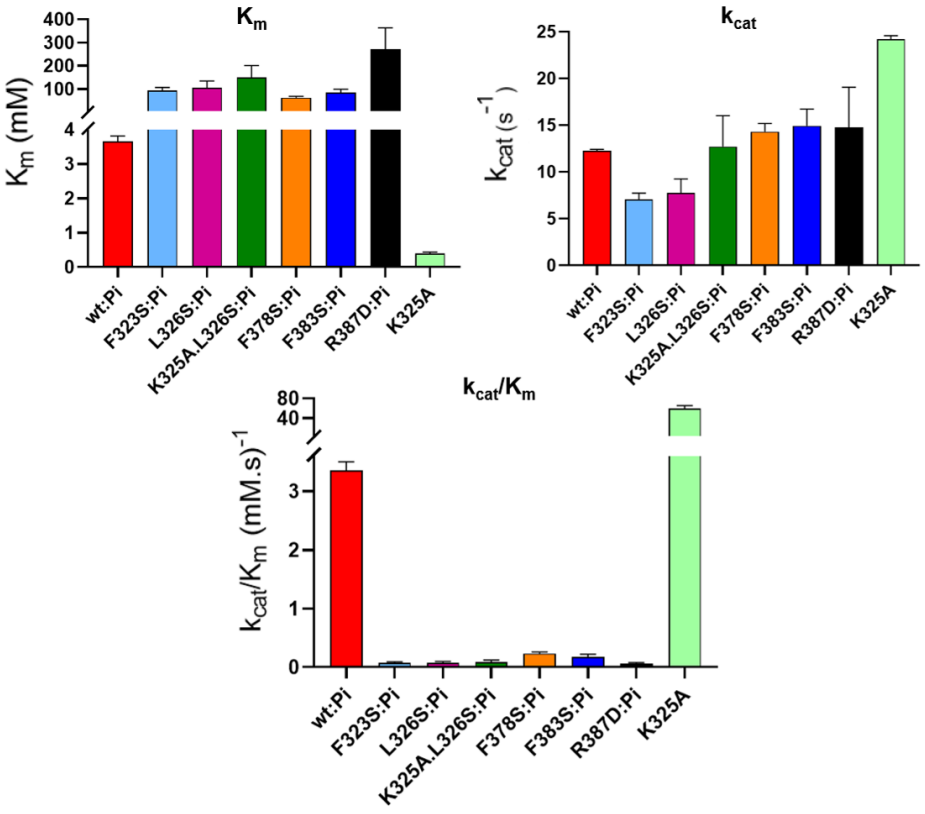

Figure 15 - Kinetic parameters for all GAC constructs. Km, kcat and kcat/Km were determined in the same conditions as shown in Figure 14.

Source: By the author.

In Figure 16 below, results are displayed showing the direct relationship between enzyme efficiency and particle size for selected mutants, confirming that disturbing a salt bridge network containing R387 and obstructing the stacking of F323 and Y471 (interactions further discussed in subsection 4.5) impairs filament formation and enzyme activation induced by phosphate. On the other hand, even in the absence of Pi, mGAC.K325A polymerizes and gains activity.

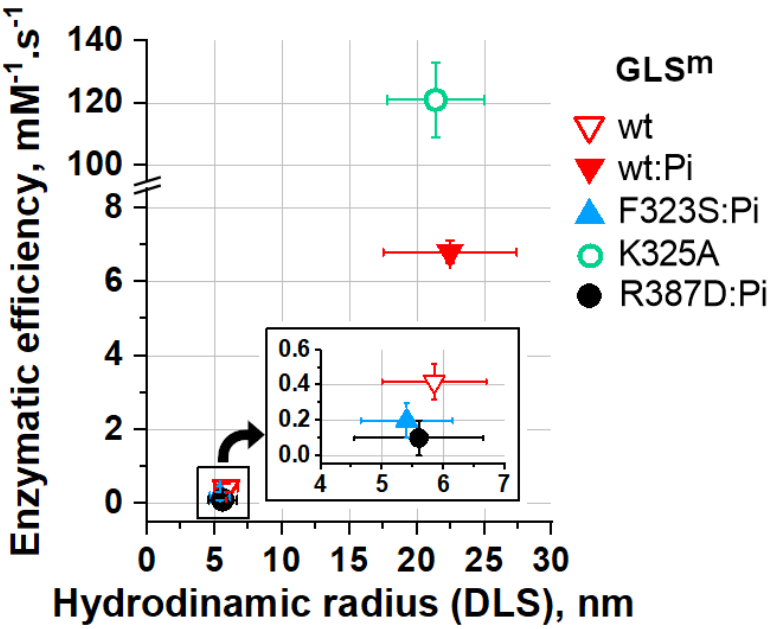

Figure 16 - Direct relationship between enzymatic efficiency and particle size. Disturbing interface interactions, as well as changing residues in the activation loop, blocked both filamentation and activity when compared to WT, while mutant K325A is the most efficient.

Source: Adapted from ADAMOSKI *et al.*[59]

In accordance with the experiments of increased Pi concentration and addition of NaCl for DLS, the same variations were implemented for the kinetic assays, as presented in Figures 17 and 18.

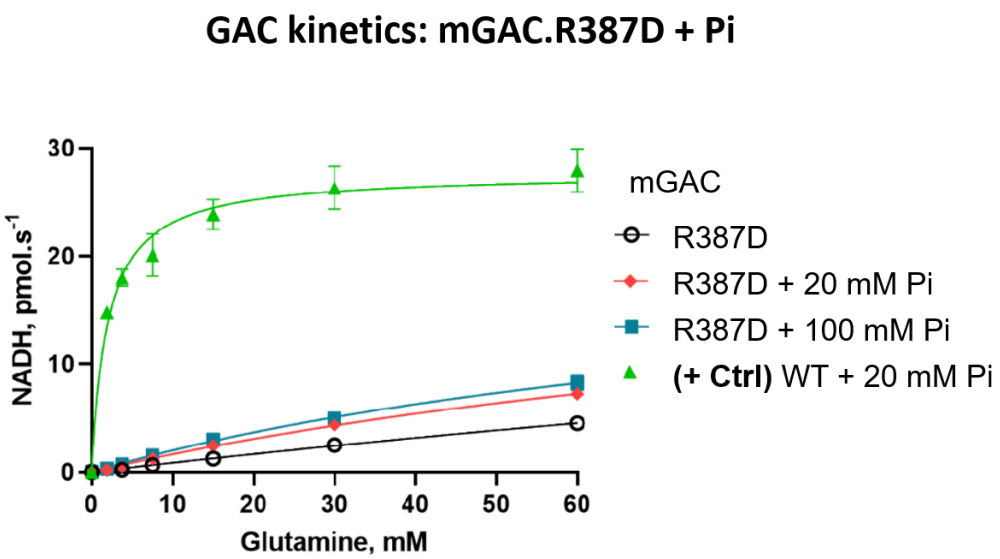

Figure 17 - Michaelis-Menten curves for mGAC.R387D, tetrameric mutant, with increasing phosphate concentrations.

Source: By the author.

In mGAC.R387D, a higher amount of Pi did not enhance enzyme activity. The efficiency of the mutant resembles tetrameric behavior, suggesting that interactions in the filament interface are essential for the stabilization of GAC in active state.

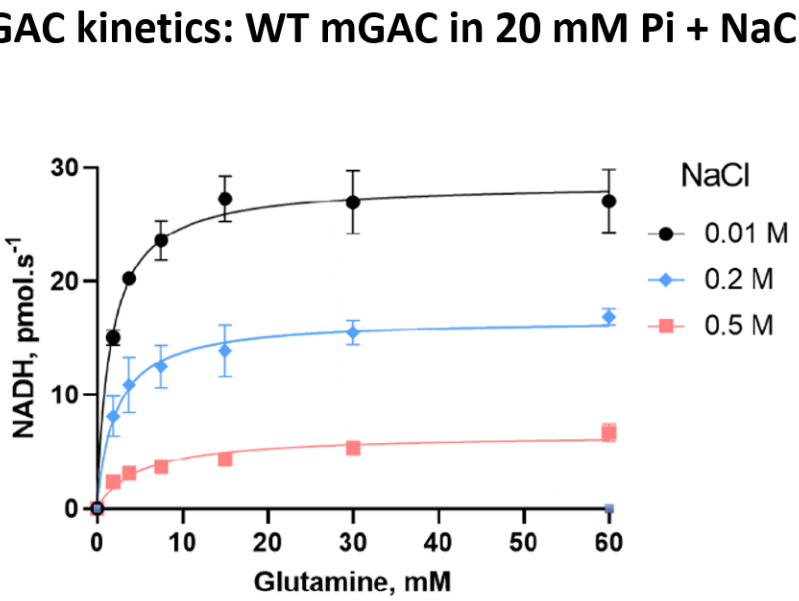

Figure 18 - Michaelis-Menten curves for WT mGAC with increasing concentrations of NaCl.

Source: By the author.

Furthermore, Figure 18 shows that, when tested with growing amount of sodium chloride, Pi-incubated WT GAC exhibited lower catalysis rates as NaCl concentration went up, despite continuing in the tetrameric form (Figure 12 in section 4.3).

4.5 GAC single-particle cryo-EM

To solve the wild-type GAC filament structure (fGAC), helical refinement was applied in combination with single-particle processing, to elucidate the GLS filament core, which is common to both GAC and KGA. A dynamic mask with symmetry expansion was used in local refinement, thereby improving global resolution from 3.4 Å to 3.1 Å.

Next, the cryo-EM map was complemented with docking of eight copies of a single glutaminase monomer (from PDB 3ss3, ligand-free GAC), followed by real space refinement.

The EF-hand-like domains at the N-terminal portion of fGAC were recognized in 2D classification and 3D reconstruction; however, they could not go through focused refinement successfully, which resulted in their omission in the final model. The unfiltered map suggests that there might be interactions between two neighboring N-terminal regions that could contribute to filament stabilization, but more experiments are necessary to validate this supposition.

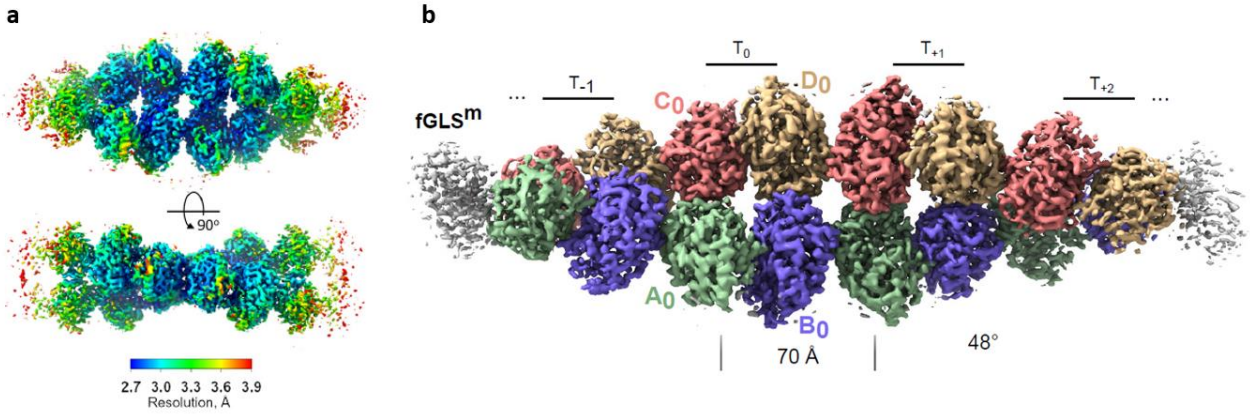

Figure 19 - fGAC model by single-particle cryo-EM. a) Local resolution of the fGAC map in orthogonal views. b) fGAC map, exhibiting helical parameters and containing four tetramers, colored by monomer.

Source: Adapted from ADAMOSKI *et al.*[59]

The helical organization is compatible with the repetition of a glutaminase tetramer (3ss3) being relocated along the longer axis of the filament, with a 70 Å rise, together with a twist of 48°. The interactions that characterize the filament are established, for the most part, by the lateral stacking of symmetric surface grooves defined by three helices from the GLS domain (N355-M370, S379-G390, and V413-I425). This model differs from the earlier proposition that the filaments were assembled by N-terminal end-to-end interactions forming each of two intertwining strands.

The activation loop in fGAC (Figure 20) is shown in a stable, closed conformation in proximity to the active site, over the substrate-binding pocket. This observation differs from the X-ray crystallography results, where the loop is unresolved, unless when bound to an allosteric inhibitor.

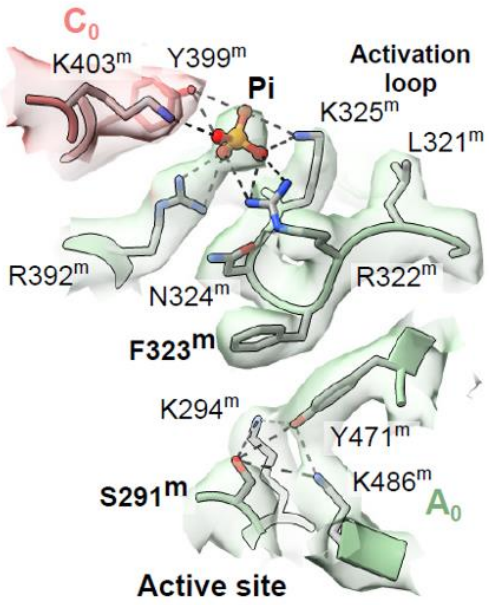

Figure 20 - **The activation loop.** The figure is colored according to the respective chain in the map. Upon the presence of Pi, the F323 residue is stacked over Y471 in the active site, thus activating the catalytic residue S291.

Source: Adapted from ADAMOSKI *et al.*[59]

The cryo-EM structure reveals a stacking of the F323 activation loop residue over Y471, which is part of the catalytic center. In this arrangement, the hydroxyl group in Y471 interacts directly with K294 and K486 forming a charge relay network, which plays a role in the polarization and activation of the S291 residue responsible for the catalytic attack to glutamine; this observation agrees with the filamentation blockage

and activity decrease caused by substitution of F323 to serine (subsections 4.3 and 4.4).

The main chain of residue L321 forms a hydrogen bond with the main chain of D472, an interaction not seen in other structures (Figure 21); for this reason, it is considered important for stability. Furthermore, the side chains of the adjacent residues L321, R322, N324, and K325 in the activation loop point in the direction opposite to F323, toward the solvent area around the tetramer interface (Figure 20).

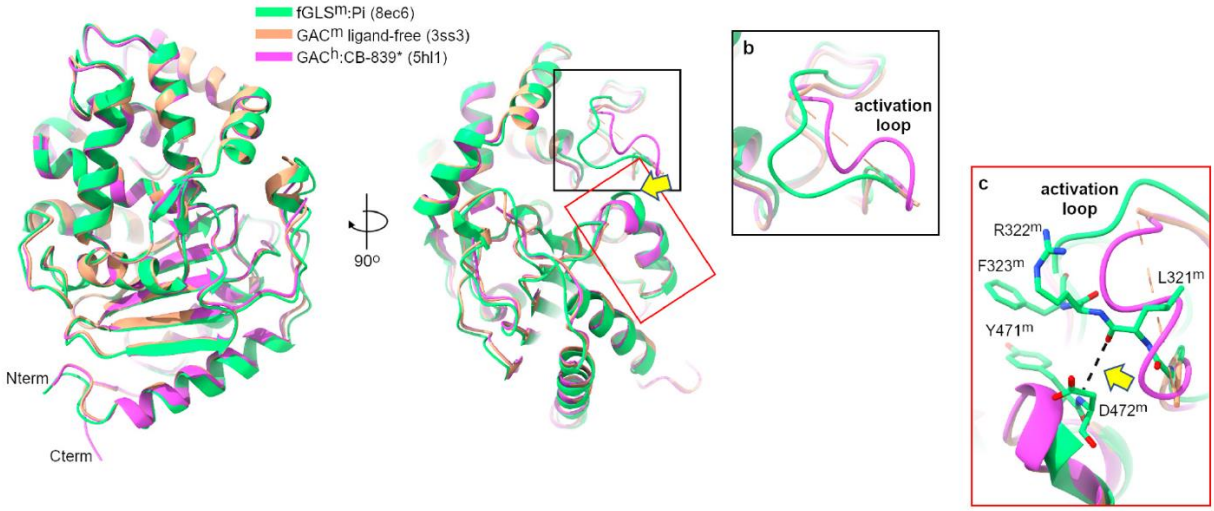

Figure 21 - Structural comparison between active fGAC and GAC. The m and h superscripts refer to the organisms of each crystal structure – mouse and human, respectively. The superposition is based on the main chain tracing. The enzyme is represented here in three states – active, from filamentous mGAC bound to Pi (green); ligand-free state of mGAC, with a dashed line in the unstructured activation loop (orange); and hGAC bound to the inhibitor CB-839 (magenta). Differences in active loop conformation are shown in more detail in (b), and the red inset in (c) shows hydrogen bonding between the main chains of L321 and D472, helping stabilize stacking between L323 and Y471.

Source: Adapted from ADAMOSKI *et al.*[59]

As was determined in the previous subsections, the introduction of the mGAC.L326S mutant hampers filamentation and Pi-induced glutamine hydrolysis (subsections 4.3 and 4.4). In contrast, a F327S substitution reported in previous works indicated gain of function. Moreover, even though mGAC.K325A makes the enzyme active and filamentous even in the absence of phosphate, the mGAC.K325A/L326S double mutant remains tetrameric and inactivated by Pi. Thus, we deduce that the distinctive stable arrangement of the activation loop of fGAC is made possible due to contribution of L326, which fills the space of a hydrophobic groove identified at the

tetramer interface, promoting the significant flip of F327 from its original position in the inactive state (Figure 22, a-c).

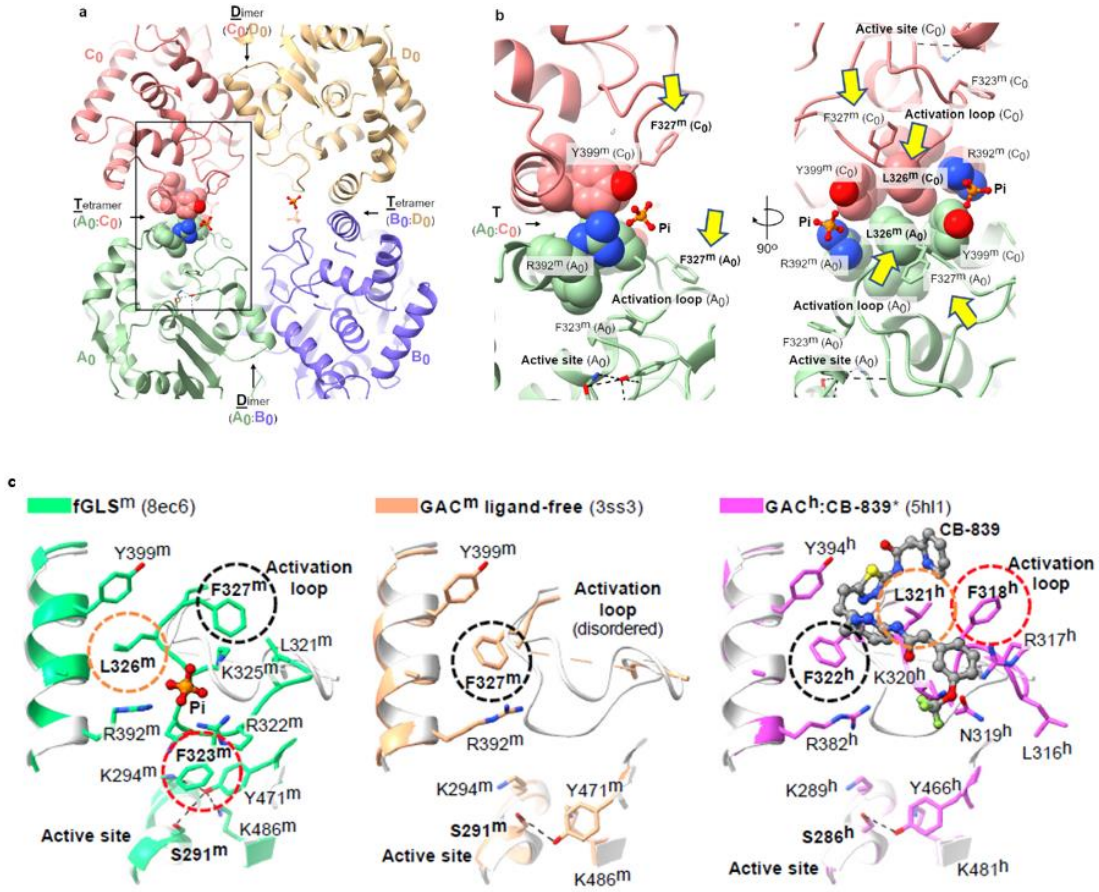

Figure 22 - Residues L326 and F327 at the tetramer interface. In (a) and (b), fGAC is shown in cartoon representation; L326 is in a hydrophobic groove (yellow arrow on the image at the right) and F327 is flipped from its original position in the inactive state. c) Structural comparison between available structures for GAC in different states. Dashed circles show conformational differences in residues from the activation loop.

Source: Adapted from ADAMOSKI *et al.* [59]

The residues R322, N324, and K325 contact Y399 and K403 from the adjacent monomer through their polar side chains, as shown in Figures 20 and 23(a), below. The area presents a foreign density in the cryo-EM map, which was regarded as a phosphate anion. Each anion is in the inner part of the tetrameric interface, where it is coordinated by 8 polar bonds. The electrostatic surface potential is changed in this region, containing an electropositive area appropriate for Pi binding, unlike the ligand-free and CB-839-bound structures, reshaping the entrance to the active site (shown by the yellow dashed lines in Figure 23(b).

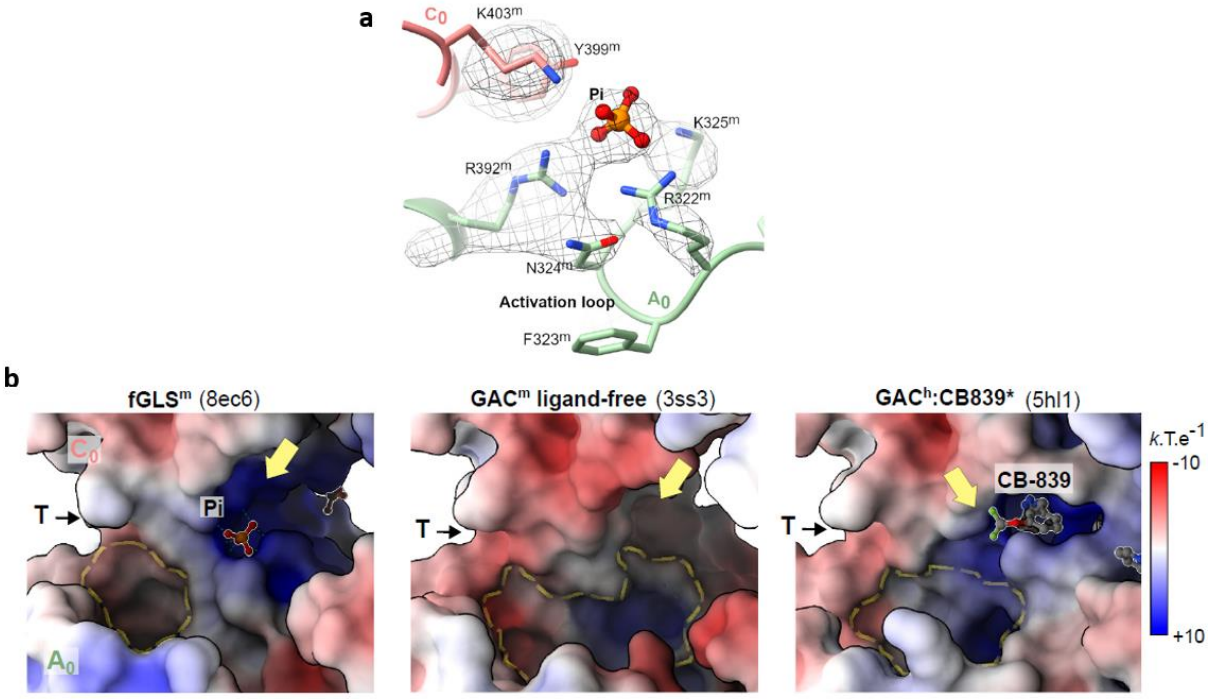

Figure 23 - Pi binding and neighboring regions. (a) shows model structures of phosphate and near densities. b) Electrostatic potential surfaces showing the positive area that allows the binding of phosphate ions. The same region is mostly negative (ligand-free) or blocked (allosteric inhibitor crystal structure) in other cases, changing the pockets available for Gln binding (yellow dashed lines).

Source: Adapted from ADAMOSKI *et al.*[59]

Although the substitution of R322 to alanine impairs Pi-induced catalysis and higher-order oligomerization, as was described by Cassago *et al.,* 2012, mGAC.K325A makes the enzyme active and filamentous even in the absence of phosphate (subsections 4.3 and 4.4); it is possible to say that the neutralization of the positive charge of K325 is crucial for glutaminase activity.

fGAC structure also gains a contribution from the lid loop (V251-D264): residue Y254 in the YIP motif from the loop is positioned toward the catalytic site, as shown in figure 24 below. Previous studies demonstrated that the YIP motif closes off the active site upon glutamine binding; hence, this finding indicates that the filamentous structure displays the GAC ready for catalysis.

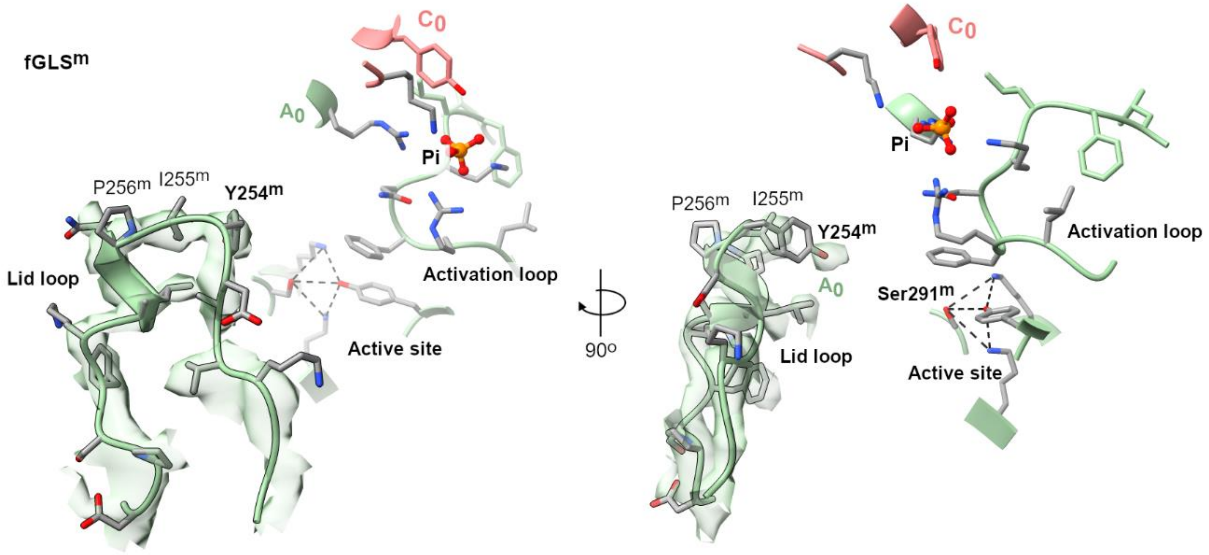

Figure 24 - Conformation of the lid loop next to the activation loop. The lid loop (V251-D264) is partially closed over the active site.

Source: Adapted from ADAMOSKI *et al.*[59]

Furthermore, we suggest that rigid body rotations around the center of mass of each monomer provoke the weakening of hydrophobic interactions at the interface, as well as disruption of essential salt bridges and hydrogen bonds in fGAC. As a result, each of the main dimer interfaces is only half as large as in the crystallographic structure (PDB 3ss3, ligand-free GAC), with a buried interface area of 740 Å^2 for fGAC as opposed to 1600 Å^2 for the tetramer. The disturbed contacts between C-terminal residues and the motion of GLS domain away from the interface enabled the appearance of a trough-like structure (Figure 25b).

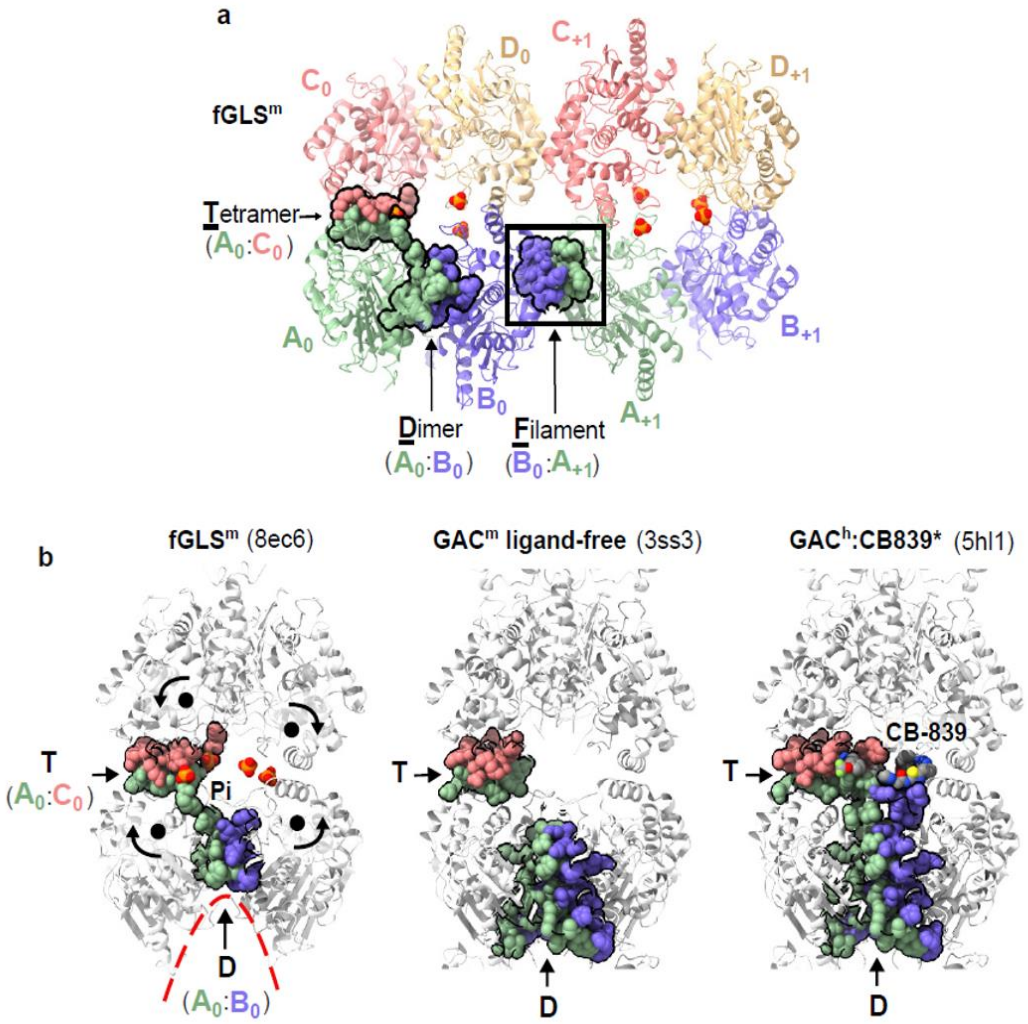

Figure 25 - Interfaces forming the filament. a) The interfaces that define dimers, tetramers, and filament (black square) are shown in space-filling representations of all atoms of the residues involved in the relevant interactions. b) Areas of the interface are changed in fGAC, or fGLS, creating a trough (D, red dashed line) resulting from monomer rotations when compared to crystal structures of ligand-free and inhibitor-bound GAC.

Source: Adapted from ADAMOSKI *et al.*[59]

PDBePISA analysis showed that, for the tetrameric interface, the area (1000 Å^2) and hydrogen bond number (6) are the same for both fGAC and ligand-free GAC, whereas filamentation weakened hydrophobic contacts by threefold.

Figure 26 shows two interacting monomers in the filamentation interface.

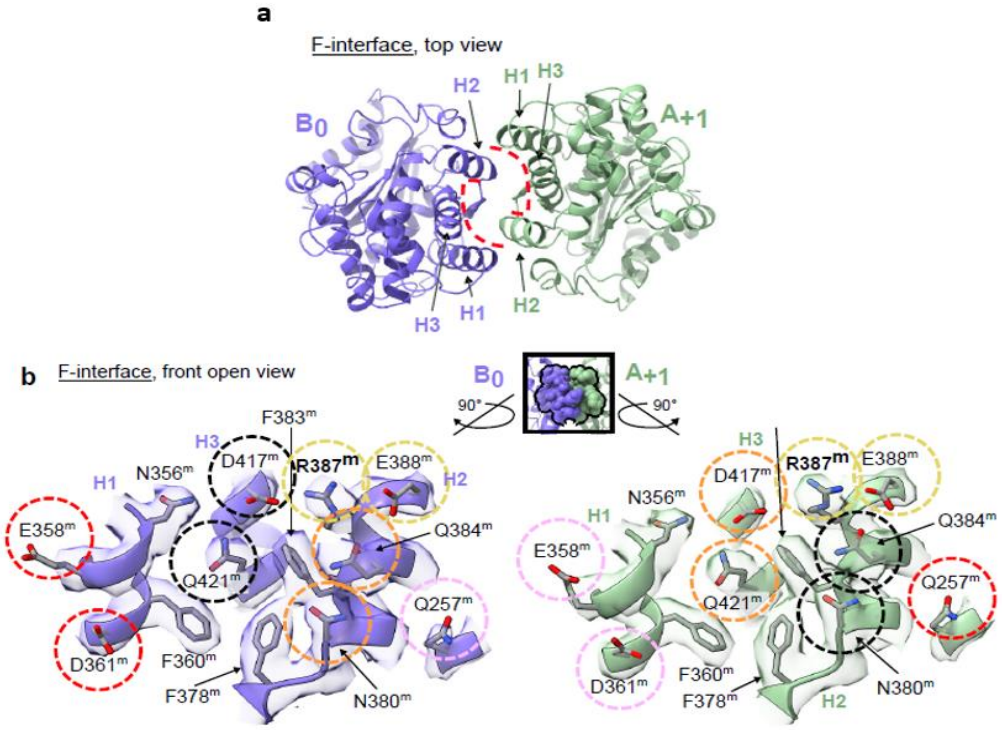

Figure 26 - Critical residues at the filament interface of fGAC. a) Top view exhibits symmetric grooves (red dashed lines) formed by helices H1 (N355-M370), H2 (S379-G390), and H3 (V413-I425). b) Front of the filament interface is exhibited in an open view. Dashed lines of the same colors indicate residues interacting with each other between the monomers.

Source: Adapted from ADAMOSKI *et al*.[59]

The disruption of the salt bridge network between R387 and E388 (Figure 26) by R387D mutation impaired filamentation and inactivated the protein. Additionally, hydrophobic interactions helped stabilize the pairs of F360, F378, and F383 shown in Figure 26; substitutions F378S and F383S obstruct glutaminase polymerization and activation (view subsections 4.3 and 4.4), demonstrating the relevance of this tetramer-tetramer interface for the process.

Based on this information, we suggest that the Pi-induced rotations of single monomers create four interaction surfaces for each tetramer-tetramer contact that characterizes the glutaminase filament.

Below, we discuss the results and propose the molecular mechanism of GAC activation induced by phosphate binding, based on our observations.

5 DISCUSSION

The formation of filamentous protein assemblies in cells occurs often during cell stress, such as in starvation, proliferation, and cell division, as a quick response to abrupt changes in metabolic demand. Therefore, enzyme filaments are generally closely linked to changes in biochemical function, acting, for instance, as a mechanism of allosteric regulation by affecting the stability of active or inactive states.[55] Furthermore, metabolic enzymes that undergo polymerization usually assemble into helical apolar filaments, lacking directionality.[56]

In fact, in a paper that has just been accepted and is in press, our group and colleagues have reported GAC filamentation within the mitochondria in glutamine-deprived cells, with morphology compatible with the cryo-EM structure described in this project. These elongated mitochondria with fGAC species were resistant to fission and protected from mitophagy during glutamine starvation, suggesting GAC filaments are important in mitochondrial dynamics.

Glutaminase C, of exclusive mitochondrial localization, is known to be the most efficient of four mammalian isozymes and is highly expressed in cancer cell lines, representing great research potential and interest. Additionally, among ions physiologically available, phosphate is vital for the majority of fundamental cellular functions such as the energy metabolism and has been shown to significantly increase GAC activity. Although structures with different ligands have been resolved, the binding and mechanism of Pi in GAC filamentation and activation has been elusive.

The DLS curves, showing size distribution as a function of hydrodynamic radius by volume, showed that mutations blocked GAC polymerization upon the presence of phosphate, in contrast with the wild-type and K325A controls, which led to a shift from tetrameric (approximately 5-6 nm radius) to filament behavior or spontaneous super-oligomerization, respectively. Moreover, even upon phosphate addition, mGAC mutants were associated with lower catalysis rates.

Consequently, we show that the amino acid interactions in the activation loop, near the catalytic pocket, and the interaction interface between tetramers are critical in the formation and stabilization of fGAC, and that this format makes the enzyme more efficient by facilitating substrate access to the active site, thus increasing turnover rate.

This is a crucial characteristic for tumor progression, especially in low nutrient environments responsible for cell stress.

The present work solves the fGAC cryo-EM structure, which shows the GAC tetramer as the helical unit. The N-terminal domains are situated on the sides, flanking the filament; they probably establish interactions that contribute to filament stability. Nevertheless, further research is necessary for detailed understanding.

The activation loop (L321-RFNKL-F327), absent in most structures because of its high dynamicity, is stabilized in fGAC and critical for the oligomerization process, enabled in great part because the locking of L326 in a hydrophobic cleft at the tetramer interface. Together with residues in the adjacent monomer, the loop forms a positively charged region where Pi is bound, followed by conformational change in the catalytic pocket where S291 is activated; one GAC tetramer accommodates four phosphate interaction sites.

The YIP motif in the distal lid loop, pointing toward the active site, is ready to lock the substrate upon binding, which occurs with high affinity.

Moreover, fGAC reveals a pivoting movement for each subunit of the glutaminase tetramer, enhancing the intertetrameric interface and shaping GAC for filamentation.

The polymerization interface is then defined mainly by side-by-side symmetrical interactions in residues (Q257, E358, D361, N380, F383, R387, E388, D417, and Q421), allowing stacking between the H1 (N355-M370), H2 (S379-G390), and H3 (V413-I425) helices (Figure 25a) forming shallow surface grooves.

The presented model differs from the one published in 2013, where the proposed GAC filament consisted of a double-stranded helix, with each strand being assembled by end-to-end associations between the N-termini tetrameric domains, which favored growth in only one direction. The structure had been solved based on transmission electron microscopy of negatively stained grids, combined with crystallography.

Based on our findings, we propose a novel mechanism for Pi-induced GAC activation, represented in Figure 27. GAC is present in inactive dimers, undergoing tetramerization upon increased protein concentration; phosphate binding promotes changes that enhance the tetramerization interface, driving a stable arrangement of the activation loop that stimulates the catalytic residue S291. Next, individual rotations in the tetramers induce the association of glutaminase and N-terminal (EF-hand-like)

domains, creating tetramer-tetramer interfaces that make GAC likely to polymerize into filaments (fGAC).

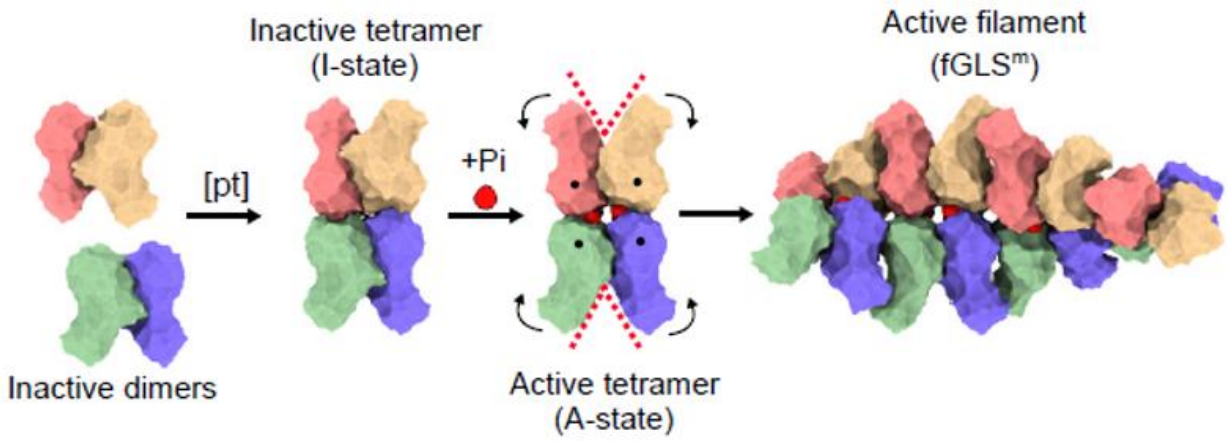

Figure 27 - GAC activation mechanism. Increasing protein concentration leads to the formation of tetramers, which can become active upon the presence of phosphate and, therefore, prone to filamentation. Inactive tetramers are common in the GLS crystal structures; however, fGAC is only observable by cryo-EM.

Source: Adapted from ADAMOSKI *et al*.[59]

It is important to note that, although phosphate drives the formation of activated fGAC, the enzyme is also active at physiological levels of glutamine (2-4 mM in cell culture media and 500-800 µM in the bloodstream[57]); therefore, we believe that a tetrameric active state (A-state), or even a short-lived filamentous state, must exist – possibly regulated by protein-protein interactions or post-translational modifications; the presence of the A-state tetramer will be studied in the existing single particle cryo-EM dataset.

Given experimental limitations, possible filament-stabilizing interactions remain to be thoroughly analyzed in the N-terminal portion of the protein (the EF-hand-like domain) in the future. Further molecular dynamics simulations could potentially provide additional insights into structural changes and interactions occurring in the polymerization process, building more substantial evidence to support the model suggested in this project.

Furthermore, research shows that many proteins in intermediary metabolism undergo alterations such as by post-translational modifications and protein-protein

interactions that might affect filamentous assembly states.[56,58] However, changes like these affecting (f)GAC were not explored for this polymerization model.

It would also be of interest to solve a cryo-EM structure for the KGA filament core, which should be similar, considering that the isozyme tends to form filaments shorter than GAC upon Pi addition, presumably affected by the C-terminal ANK repeats.

6 CONCLUSION

This project sought to explore the molecular determinants of GAC filamentation. By introducing site-directed mutations, our aim was to identify how key residues could affect the process of higher-order oligomerization correlated with enzymatic efficiency, successfully assessed by biophysical and biochemical experiments.

Additionally, we solved a novel cryo-EM structure of fGAC at 3.1 Å global resolution, disclosing an unprecedented, detailed view of the interactions defining protein-protein interfaces and conformational changes influencing the remodeling of the catalytic pocket upon the presence of phosphate inducer. Although fGAC tetramers are similar to the crystallographic ones released previously, they are stacked into a 48°-twisted filament with a 70 Å rise and present a stable activation loop leading to the highly efficient fGAC, important especially during glutamine deprivation.

Furthermore, it is pertinent to perform new experiments in order to uncover interactions in the N-terminal domains, which might also play an important role in fGAC stabilization.

In conclusion, we propose a mechanism driving the protein from inactive dimers to the hyperactive filaments, emphasizing the link between GAC oligomerization and activity. This work provides valuable insights into glutaminase mechanisms in health and disease, fostering future research developments.

REFERENCES

1 FERLAY, J. *et al.* Cancer statistics for the year 2020: an overview. **International Journal of Cancer**, v. 149, n. 4, p. 778-789, Apr. 2021.

2 THUN, M. J. *et al.* The global burden of cancer: priorities for prevention. **Carcinogenesis**, v. 31, n. 1, p. 100–110, Nov. 2009.

3 MATTIUZZI, C.; LIPPI, G. Current cancer epidemiology. **Journal of Epidemiology and Global Health**, v. 9, n. 4, p. 217–222, Dec. 2019.

4 HANAHAN, D.; WEINBERG, R. A. The hallmarks of cancer. **Cell**, v. 100, n. 1, p. 57–70, Jan. 2000.

5 HANAHAN, D.; WEINBERG, R. A. Hallmarks of cancer: the next generation. **Cell**, v. 144, n. 5, p. 646–674, Mar. 2011.

6 HANAHAN, D. Hallmarks of cancer: new dimensions. **Cancer Discovery**, v. 12, n. 1, p. 31–46, Jan. 2022.

7 NISHIDA, N. *et al*. Angiogenesis in cancer. **Vascular Health and Risk Management**, v. 2, n. 3, p. 213–219, Aug. 2006.

8 YOO, H. C. *et al*. Glutamine reliance in cell metabolism. **Experimental & Molecular Medicine**, v. 52, n. 9, p. 1496–1516, Sept. 2020.

9 YANG, L.; VENNETI, S.; NAGRATH, D. Glutaminolysis: a hallmark of cancer metabolism. **Annual Review of Biomedical Engineering**, v. 19, n. 1, p. 163–194, June 2017.

10 PHAN, L. M.; YEUNG, S.-C. J.; LEE, M.-H. Cancer metabolic reprogramming: importance, main features, and potentials for precise targeted anti-cancer therapies. **Cancer Biology & Medicine**, v. 11, n. 1, p. 1–19, 2014.

11 DEBERARDINIS, R. J.; CHANDEL, N. S. Fundamentals of cancer metabolism. **Science Advances**, v. 2, n. 5, p. e1600200, May 2016.

12 PAVLOVA, N. N.; THOMPSON, C. B. The emerging hallmarks of cancer metabolism. **Cell Metabolism**, v. 23, n. 1, p. 27–47, Jan. 2016.

13 WARBURG, O. The metabolism of carcinoma cells. **Journal of Cancer Research**, v. 9, n. 1, p. 148–163, Mar. 1925.

14 WARBURG, O. The metabolism of tumors in the body. **Journal of General Physiology**, v. 8, n. 6, p. 519–530, Mar. 1927.

15 LIBERTI, M. V.; LOCASALE, J. W. The Warburg effect: how does it benefit cancer cells? **Trends in Biochemical Sciences**, v. 41, n. 3, p. 211–218, Mar. 2016.

16 BOSE, S.; ZHANG, C.; LE, A. Glucose metabolism in cancer: the Warburg effect and beyond. **Advances in Experimental Medicine and Biology**, p. 3–15, 2021. DOI: 10.1007/978-3-030-65768-0_1

17 VANDER HEIDEN, M. G.; CANTLEY, L. C.; THOMPSON, C. B. Understanding the Warburg effect: the metabolic requirements of cell proliferation. **Science**, v. 324, n. 5930, p. 1029–1033, May 2009.

18 HSU, P. P.; SABATINI, D. M. Cancer cell metabolism: Warburg and beyond. **Cell**, v. 134, n. 5, p. 703–707, Sept. 2008.

19 DEBERARDINIS, R. J.; CHENG, T. Q's next: the diverse functions of glutamine in metabolism, cell biology and cancer. **Oncogene**, v. 29, n. 3, p. 313–324, Nov. 2009.

20 ALTMAN, B. J.; STINE, Z. E.; DANG, C. V. From Krebs to clinic: glutamine metabolism to cancer therapy. **Nature Reviews Cancer**, v. 16, n. 10, p. 619–634, July 2016.

21 CLUNTUN, A. A. *et al*. Glutamine metabolism in cancer: understanding the heterogeneity. **Trends in Cancer**, v. 3, n. 3, p. 169–180, Mar. 2017.

22 WISE, D. R.; THOMPSON, C. B. Glutamine addiction: a new therapeutic target in cancer. **Trends in Biochemical Sciences**, v. 35, n. 8, p. 427–433, Aug. 2010.

23 BHUTIA, Y. D.; GANAPATHY, V. Glutamine transporters in mammalian cells and their functions in physiology and cancer. **Biochimica et Biophysica Acta (BBA)** - molecular cell research, v. 1863, n. 10, p. 2531–2539, Oct. 2016.

24 YOO, H. C. *et al*. A variant of SLC1A5 Is a mitochondrial glutamine transporter for metabolic reprogramming in cancer cells. **Cell Metabolism**, v. 31, n. 2, p. 267-283.e12, Feb. 2020.

25 KREBS, H. A. Metabolism of amino-acids. **Biochemical Journal**, v. 29, n. 8, p. 1951–1969, Aug. 1935.

26 SHIJIE, J. *et al.* Blockade of glutamate release from microglia attenuates experimental autoimmune encephalomyelitis in mice. **Tohoku Journal of Experimental Medicine**, v. 217, n. 2, p. 87–92, 2009.

27 DING, L. *et al.* Glutaminase in microglia: a novel regulator of neuroinflammation. **Brain, Behavior, and Immunity**, v.92, p. 139- 156, Feb. 2021. DOI: 10.1016/j.bbi.2020.11.038.

28 GAO, G. *et al*. Glutaminase 1 regulates neuroinflammation after cerebral ischemia through enhancing microglial activation and pro-inflammatory exosome release. **Frontiers in Immunology**, v. 11, Feb. 2020. DOI: 10.3389/fimmu.2020.00161.

29 WANG, J. B. *et al.* Targeting mitochondrial glutaminase activity inhibits oncogenic transformation. **Cancer Cell**, v. 18, n. 3, p. 207–219, Sept. 2010.

30 KAROLINE, R. *et al.* High-throughput screening reveals new glutaminase inhibitor molecules. **ACS Pharmacology & Translational Science**, v. 4, n. 6, p. 1849–1866, Dec. 2021.

31 GROSS, M. I. *et al.* Antitumor activity of the glutaminase inhibitor CB-839 in triple-negative breast cancer. **Molecular Cancer Therapeutics**, v. 13, n. 4, p. 890–901, Feb. 2014.

32 FERREIRA, A. T*. et al.* Active glutaminase C self-assembles into a supratetrameric oligomer that Can Be disrupted by an allosteric inhibitor**. Journal of Biological Chemistry,** v. 288, n. 39, p. 28009–28020, Sept. 2013.

33 KATT, W. P.; LUKEY, M. J.; CERIONE, R. A. A tale of two glutaminases: homologous enzymes with distinct roles in tumorigenesis. **Future Medicinal Chemistry**, v. 9, n. 2, p. 223–243, 2017.

34 ELGADI, K. M*. et al.* Cloning and analysis of unique human glutaminase isoforms generated by tissue-specific alternative splicing. **Physiological Genomics**, v. 1, n. 2, p. 51–62, 31 ago. 1999.

35 CAMPOS-SANDOVAL, J. A*. et al.* Glutaminases in brain: multiple isoforms for many purposes. **Neurochemistry International**, v. 88, p. 1–5, set. 2015.

36 GOMEZ-FABRE, P. *et al*. Molecular cloning, sequencing and expression studies of the human breast cancer cell glutaminase. **Biochemical Journal**, v. 345, Pt. 2, p. 365, 2000.

37 WANG, Y. *et al.* Glutaminase C overexpression in the brain induces learning deficits, synaptic dysfunctions, and neuroinflammation in mice. **Brain Behavior and Immunity**, v. 66, p. 135–145, Nov. 2017. DOI: 10.1016/j.bbi.2017.06.007.

38 TURNER, A.; MCGIVAN, J. D. Glutaminase isoform expression in cell lines derived from human colorectal adenomas and carcinomas. **Biochemical Journal**, v. 370, n. 2, p. 403–408, Mar. 2003.

39 SZELIGA, M. *et al.* Relative expression of mRNAS coding for glutaminase isoforms in CNS tissues and CNS tumors. **Neurochemical Research**, v. 33, n. 5, p. 808–813, Oct. 2007.

40 GAO, P. *et al. c*-Myc suppression of miR-23a/b enhances mitochondrial glutaminase expression and glutamine metabolism. **Nature**, v. 458, n. 7239, p. 762–765, Feb. 2009.

41 LUKEY, M. J*. et al.* The oncogenic transcription factor c-Jun regulates glutaminase expression and sensitizes cells to glutaminase-targeted therapy. **Nature Communications**, v. 7, Apr. 2016. DOI: 10.1038/ncomms11321.

42 CHUNG-BOK, M. I. *et al.* Rat hepatic glutaminase: identification of the full coding sequence and characterization of a functional promoter. **Biochemical Journal**, v. 324, n. 1, p. 193–200, May 1997.

43 OLALLA, L. *et al.* Nuclear localization of L-type glutaminase in mammalian brain. **Journal of Biological Chemistry**, v. 277, n. 41, p. 38939–38944, Oct. 2002.

44 MÁRQUEZ, J. *et al.* Glutaminase: a multifaceted protein not only involved in generating glutamate. **Neurochemistry International**, v. 48, n. 6-7, p. 465–471, May 2006.

45 DIAS, M. M. *et al.* GLS2 is protumorigenic in breast cancers. **Oncogene**, v. 39, n. 3, p. 690–702, Jan. 2020.

46 PRIVES, C. *et al.* GLS2 Is a tumor suppressor and a regulator of ferroptosis in hepatocellular carcinoma. **Cancer Research**, v. 82, n. 18, p. 3209–3222, July 2022.

47 PASQUALI, C. C. *et al*. The origin and evolution of human glutaminases and their atypical C-terminal ankyrin repeats. **Journal of Biological Chemistry**, v. 292, n. 27, p. 11572–11585, July 2017.

48 LEWIT-BENTLEY, A.; RÉTY, S. EF-hand calcium-binding proteins. **Current Opinion in Structural Biology**, v. 10, n. 6, p. 637–643, 2000.

49 GOMES, A. V.; POTTER, J. D.; SZCZESNA-CORDARY, D. The role of troponins in muscle contraction. **IUBMB Life**, v. 54, n. 6, p. 323–333, 2002.

50 STEVENS, F. C. Calmodulin: an introduction. **Canadian Journal of Biochemistry and Cell Biology**, v. 61, n. 8, p. 906–910, Aug. 1983.

51 CASSAGO, A. *et al.* Mitochondrial localization and structure-based phosphate activation mechanism of Glutaminase C with implications for cancer metabolism. **Proceedings of the National Academy of Sciences**, v. 109, n. 4, p. 1092–1097, Jan. 2012.

52 GORMAN, M. W. *et al.* Inorganic phosphate as regulator of adenosine formation in isolated guinea pig hearts. **American Journal of Physiology -** heart and circulatory physiology, v. 272, n. 2, p. H913–H920, Feb. 1997.

53 BOUHAMIDA, E. *et al.* The interplay of hypoxia signaling on mitochondrial dysfunction and inflammation in cardiovascular diseases and cancer: from molecular mechanisms to therapeutic approaches. **Biology**, v. 11, n. 2, p. 300, Feb. 2022.

54 LI, Y. *et al*. Mechanistic basis of glutaminase activation. **Journal of Biological Chemistry**, v. 291, n. 40, p. 20900–20910, 2016.

55 LYNCH, E. M.; KOLLMAN, J. M.; WEBB, B. A. Filament formation by metabolic enzymes - a new twist on regulation. **Current Opinion in Cell Biology**, v. 66, p. 28–33, Oct. 2020. DOI: 10.1016/j.ceb.2020.04.006.

56 HVORECNY, K. L.; KOLLMAN, J. M. Greater than the sum of parts: mechanisms of metabolic regulation by enzyme filaments. **Current Opinion in Structural Biology**, v. 79, p. 102530, 2023. DOI: 10.1016/j.sbi.2023.102530

57 CRUZAT, V. *et al.* Glutamine: metabolism and immune function, supplementation and clinical translation. **Nutrients**, v. 10, n. 11, p. 1564, Nov. 2018.

58 PARK, C. K.; HORTON, N. C. Structures, functions, and mechanisms of filament forming enzymes: a renaissance of enzyme filamentation. **Biophysical Reviews**, v. 11, n. 6, p. 927–994, 2019.

59 ADAMOSKI, D. *et al*. Molecular mechanism of glutaminase activation through filamentation and the role of filaments in mitophagy protection. **Nature Structural and Molecular Biology**. In press.